The J6/JFH1-P47 strain of HCV used in this study possesses adaptive mutations compared to the original strain (J6/JFH1-P1). Therefore, we compared the impacts of the two strains on cell viability/proliferation and DNA fragmentation. While both strains caused inhibition of cell proliferation and an increase in DNA fragmentation, J6/JFH1-P47 appeared to exert a stronger cytopathic effect than J6/JFH-P1 (data not shown).

To further verify that HCV infection induces apoptotic cell death, we analyzed caspase 3 activities in HCV-infected Huh7.5 cells and the mock-infected control. As shown in Fig. 2A, caspase 3 activities in HCV-infected cells increased to levels that were 2.2, 6.0, and 12 times higher than that in the control cells at 2, 4, and 6 days postinfection, respectively. We also examined HCV-induced caspase 3 activation by immunoblot analysis. Activation of caspase 3 requires proteolytic processing of its inactive proenzyme into the active 17-kDa and 12-kDa subunit proteins. The anti-caspase 3 antibody used in this analysis recognizes 35-kDa procaspase 3 and the 17-kDa subunit protein. At 6 days postinfection, activated caspase 3 was detected in HCV-infected cells but not in the mock-infected control (Fig. 2B, second row from the top). Analysis of the death substrate PARP, which is a key substrate for active caspase 3 (61), also demonstrated that the uncleaved PARP (116 kDa) was proteolytically cleaved to generate the 89-kDa fragment in HCV-infected cells but not in the mock-infected control (Fig. 2B, third row). Cleavage of PARP facilitates cellular disassembly and serves as a marker of cells undergoing apoptosis (44).

In order to further confirm these observations, indirect immunofluorescence staining was performed by using an anti-active caspase 3 antibody that specifically recognizes the newly exposed C terminus of the 17-kDa fragment of caspase 3 but not the inactive precursor form. As shown in Fig. 2C, the activated form of caspase 3 was clearly observed in HCV-infected cells but not in the mock-infected control at 6 days postinfection. The activation of caspase 3 was observed also at 4 days postinfection (data not shown). We found that caspase 3 activation was detectable in 12% and 21% of HCV antigen-positive cells at 4 and 6 days postinfection, respectively, whereas it was detectable only minimally in mock-infected cells at the same time points (Fig. 2D). These results strongly suggest that HCV-induced cell death is caused by caspase 3-dependent apoptosis. We also observed nuclear translocation of active caspase 3 in HCV-infected cells (Fig. 2E). This result is consistent with previous reports (28, 70) that activated caspase 3 is located not only in the cytoplasm but also in the nuclei of apoptotic cells. Concomitantly, nuclear condensation and shrinkage were clearly observed in the caspase 3-activated cells. As the activation and nuclear translocation of caspase 3 occur before the appearance of the nuclear change, not all caspase 3-activated cells exhibited the typical nuclear changes. Taken together, these results indicate that HCV-induced apoptosis is associated with activation and nuclear translocation of caspase 3.

HCV infection induces the activation of the proapoptotic protein Bax. The proteins of the Bcl-2 family are known to directly regulate mitochondrial membrane permeability and induction of apoptosis (63). Therefore, we examined the expression levels of proapoptotic proteins, such as Bax and Bak, and antiapoptotic protein Bcl-2 in HCV-infected Huh7.5 cells and the mock-infected control. The result showed that expression levels of Bak or Bcl-2 did not differ significantly between HCV-infected cells and the control. Interestingly, however, Bax accumulated on the mitochondria in HCV-infected cells to a larger extent than in the mock-infected control (Fig. 3A), with the average amount of mitochondrion-associated Bax in HCV-infected cells being 2.7 times larger than that in the control cells at 6 days postinfection (Fig. 3B).

In response to apoptotic stimuli, Bax undergoes a conformational change to expose its N and C termini, which facilitates translocation of the protein to the mitochondrial outer membrane (32). Thus, the conformational change of Bax represents a key step for its activation and subsequent apoptosis. We therefore investigated the possible conformational change of Bax in HCV-infected cells by using a conformation-specific NT antibody that specifically recognizes the Bax protein with an exposed N terminus. As shown in Fig. 3C, Bax staining with the conformation-specific NT antibody was readily detectable in HCV-infected cells at 6 days postinfection whereas there was no detectable staining with the same antibody in the mock-infected control. Moreover, the activated Bax was shown to be colocalized with MitoTracker, a marker for mitochondria, in HCV-infected cells. The conformational change of Bax was observed in 10% and 15% of HCV-infected cells at 4 and 6 days postinfection, respectively (Fig. 3D). This result was consistent with what was observed for caspase 3 activation in HCV-infected cells (Fig. 2D). Taken together, these results suggest that HCV infection triggers conformational change and mitochondrial accumulation of Bax, which lead to the activation of the mitochondrial apoptotic pathway.

HCV infection induces the disruption of the mitochondrial transmembrane potential, release of cytochrome *c* from mitochondria, and activation of caspase 9. The accumulation of Bax on the mitochondria is known to decrease the mitochondrial transmembrane potential and increase its permeability, which result in the release of cytochrome *c* and other key molecules from the mitochondria to the cytoplasm to activate caspase 9. Therefore, we examined the possible effect of HCV infection on mitochondrial transmembrane potential in Huh7.5 cells. Disruption of the mitochondrial transmembrane potential was indicated by decreased Rho123 retention and, hence, decreased fluorescence. As shown in Fig. 4, HCV-infected cells showed ~50% and ~70% reductions in Rho123 fluorescence intensity compared with the mock-infected control at 4 and 6 days postinfection, respectively.

Recent studies have indicated that loss of mitochondrial membrane potential leads to mitochondrial swelling, which is often associated with cell injury (27, 50). Also, we and other investigators have reported that HCV NS4A (43), core (53), and p7 (22) target mitochondria. We therefore analyzed the effect of HCV infection on mitochondrial morphology. Confocal fluorescence microscopic analysis using MitoTracker revealed that mitochondria began to undergo morphological changes at 4 days postinfection and that approximately 40% of HCV-infected cells exhibited mitochondrial swelling and/or aggregation compared with the mock-infected control at 6 days postinfection (Fig. 5A and B). It should also be noted that mitochondrial swelling and/or aggregation was seen in a region different from the "membranous web," where the HCV replication complexes accumulate to show stronger expression of

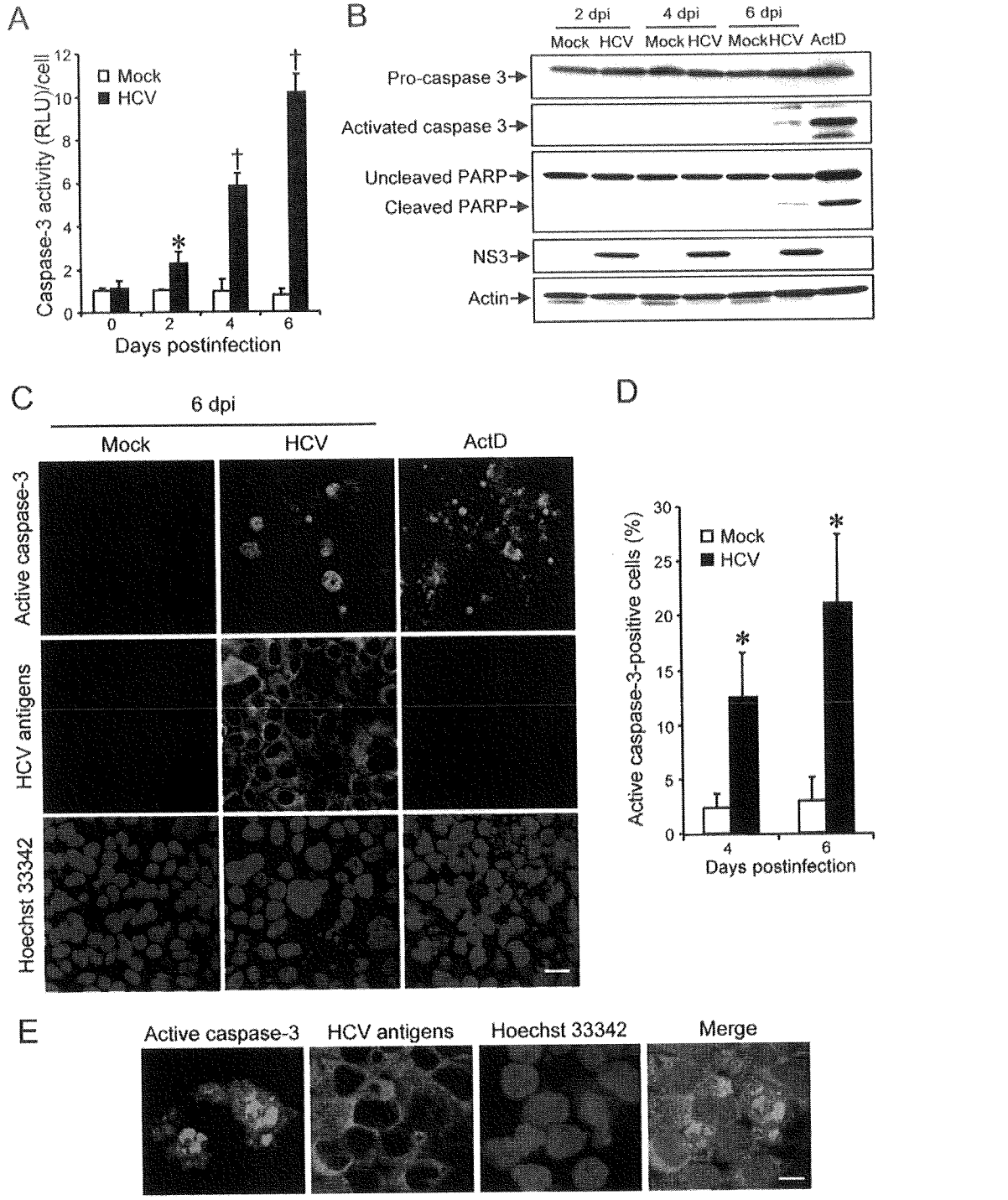

FIG. 2. HCV infection activates caspase 3 in Huh7.5 cells. (A) Caspase 3 activities in cells infected with HCV and mock-infected controls. The caspase 3 activity of the control cells at day 0 postinfection was arbitrarily expressed as 1.0. *, $P < 0.05$; †, $P < 0.01$ (compared with the control). Data represent means ± standard deviations (SD) of three independent experiments. (B) Immunoblot analysis to detect the activated form of caspase 3 (~17 kDa) and cleavage product of PARP (~85 kDa) in HCV-infected cells and the mock-infected control at 2, 4, and 6 days postinfection (dpi). Huh7.5 cells treated with actinomycin D (ActD; 50 ng/ml) for 30 h served as a positive control. Amounts of actin were measured as an internal control to verify an equal amount of sample loading. (C) Huh7.5 cells infected with HCV or mock infected were subjected to indirect immunofluorescence analysis at 6 dpi. Cells treated with ActD (50 ng/ml) for 30 h served as a positive control. After fixation and permeabilization, the cells were incubated with anti-active caspase 3 rabbit polyclonal antibody followed by Cy3-labeled donkey anti-rabbit IgG (top) and with an HCV-infected patient's serum followed by FITC-labeled goat anti-human IgG (middle). The cells were then stained with Hoechst 33342 for the nuclei (bottom). Scale bar, 20 μm. (D) Quantification of active caspase 3-expressing cells. The percentages of cells expressing active caspase 3 were determined for HCV-infected cultures and mock-infected controls. Data represent means ± SD of three independent experiments. *, $P < 0.05$, compared with the control. (E) Nuclear translocation of active caspase 3 in HCV-infected cells. Subcellular localization of active caspase 3 in HCV-infected cells was examined by indirect immunofluorescence analysis at 6 days postinfection as described in the legend for panel C. Scale bar, 5 μm.

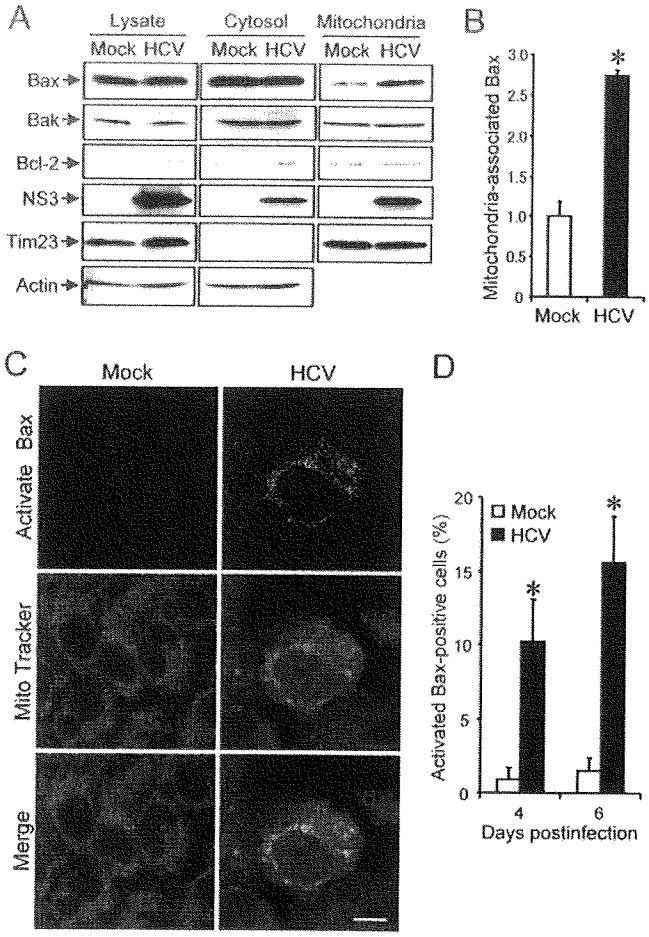

FIG. 3. HCV infection induces Bax activation in Huh7.5 cells. (A) Accumulation of Bax on the mitochondria in HCV-infected Huh7.5 cells. Cytosolic and mitochondrial fractions as well as whole-cell lysates were prepared from HCV-infected cells and the mock-infected control at 6 days postinfection and analyzed by immunoblotting using antibodies against Bax, Bak, Bcl-2, NS3, Tim23, and actin. Amounts of Tim23, a mitochondrion-specific protein, were measured to verify equal amounts of mitochondrial fractions. Amounts of actin were measured to verify equal amounts of whole-cell lysates and cytosolic fractions. (B) The intensities of the bands of mitochondrion-associated Bax in HCV-infected cells and the mock-infected control were quantified. The intensity of the mock-infected control was arbitrarily expressed as 1.0. Data represent means ± standard deviations (SD) of three independent experiments. *, $P < 0.01$, compared with the control. (C) Conformational change of Bax in HCV-infected cells. Huh7.5 cells infected with HCV and the mock-infected control were subjected to indirect immunofluorescence analysis at 6 days postinfection. After incubation with MitoTracker (middle row), the cells were incubated with an antibody specific for the N terminus of Bax (NT antibody), followed by Alexa Fluor 488-labeled goat anti-rabbit IgG (top row). Merged images are shown on the bottom. Scale bar, 10 μm. (D) Quantification of activated Bax-positive cells. The percentages of cells expressing activated Bax were determined for HCV-infected cultures and the mock-infected control. Data represent means ± SD of three independent experiments. *, $P < 0.01$, compared with the control.

HCV antigens. This observation implies the possibility that an indirect effect(s) of HCV infection, in addition to a direct effect of an HCV protein, as observed for NS3/4A (43), is involved in mitochondrial swelling and/or aggregation.

Electron microscopic analysis also demonstrated swelling and structural alterations of mitochondria in HCV-infected cells, whereas mitochondria remained intact in the mock-infected control (Fig. 5C). This result suggests a detrimental effect of HCV infection on the volume homeostasis and morphology of mitochondria and is consistent with previous observations that liver tissues from HCV-infected patients showed morphological changes in mitochondria (3).

Mitochondrial swelling and the morphological change of mitochondrial cristae are associated with cytochrome *c* release (27, 54). We then examined the effect of HCV infection on cytochrome *c* release in Huh7.5 cells. The result clearly demonstrated cytochrome *c* release from the mitochondria to the cytoplasm in HCV-infected cells but not in the mock-infected control (Fig. 6A). The release of cytochrome *c* from mitochondria is known to induce activation of caspase 9 (31). We then analyzed caspase 9 activities in the cells. As shown in Fig. 6B, caspase 9 activities in HCV-infected cells increased to levels that were ca. five times higher than that in the control cells at 4 and 6 days postinfection.

HCV infection induces a marginal degree of caspase 8 activation. In addition to the mitochondrial death (intrinsic) pathway described above, the extrinsic cell death pathway, which is initiated by the TNF family members and mediated by activated caspase 8 (31, 62), is also the focus of attention in the study of apoptosis. Therefore, we examined caspase 8 activities in HCV-infected cells and the mock-infected control. As shown in Fig. 6C, caspase 8 activities in HCV-infected cells increased to a level that was ca. two times higher than that in the control cells at 4 and 6 days postinfection. This increase was much smaller than that observed for caspase 9 activation (Fig. 6B).

HCV infection induces increased production of mitochondrial reactive oxygen species (ROS). The production of ROS, such as superoxide, by mitochondria is the major cause of cellular oxidative stress (8), and a possible link between ROS production and Bax activation has been reported (18, 42). Therefore, we next examined the mitochondrial ROS production in HCV- and mock-infected cells by using MitoSOX, a fluorescent probe specific for superoxide that selectively accumulates in the mitochondrial compartment. As shown in Fig. 7A and B, approximately 25% of HCV-infected cells displayed a much higher signal than did the mock-infected control. This result suggests that oxidative stress is induced by HCV infection.

HCV infection does not induce ER stress. It is well known that HCV nonstructural proteins form the replication complex on the endoplasmic reticulum (ER) membrane (4, 19, 39, 46). It was recently reported that HCV infection (55) as well as the transfection of the full-length HCV replicon (17) and the expression of the entire HCV polyprotein (14) induced an ER stress response. Therefore, we tested whether HCV infection in our system induces ER stress. We adopted increased expression of GRP78 and GRP94 as indicators of ER stress (34) and, as a positive control, used tunicamycin to induce ER stress (20, 25). As had been expected, the expression levels of GRP78 and GRP94 were markedly increased in Huh7.5 cells when cells were treated with tunicamycin for 48 h (Fig. 8, right). On the other hand, HCV infection did not alter expression levels of GRP78 or GRP94 at 2, 4, or 6 days postinfection compared

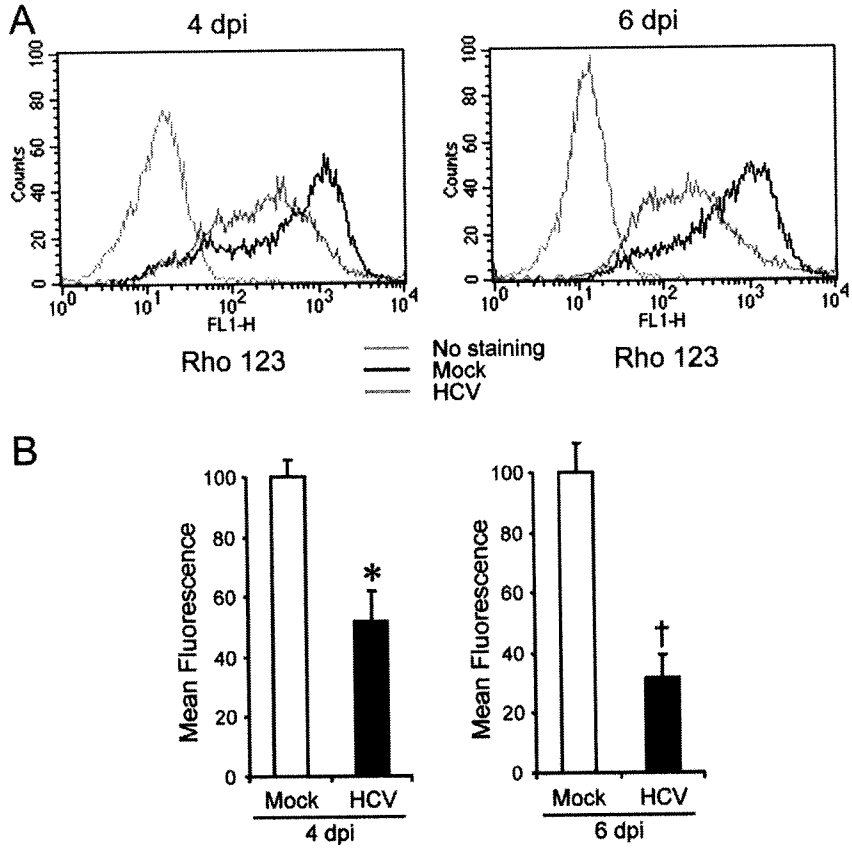

FIG. 4. HCV infection induces disruption of the mitochondrial transmembrane potential in Huh7.5 cells. (A) Huh7.5 cells infected with HCV and the mock-infected control were stained with Rho123 and subjected to flow cytometric analysis to measure the mitochondrial transmembrane potential at 4 and 6 days postinfection (dpi). The red and black lines represent Rho123 staining of HCV-infected cells and the mock-infected control, respectively. The green profiles represent staining of the cells with PBS alone. (B) Mean fluorescence intensities of HCV-infected cells and the mock-infected control at 4 and 6 dpi. Data represent means ± standard deviations (SD) of three independent experiments. *, $P < 0.05$; †, $P < 0.01$ (compared with the control).

with those for the mock-infected control (Fig. 8). This result suggests that ER stress, if there is any, is marginal and does not play an important role in HCV-induced apoptosis in Huh7.5 cells.

DISCUSSION

The mitochondrion is an important organelle for cell survival and death and plays a crucial role in regulating apoptosis. An increasing body of evidence suggests that apoptosis occurs in the livers of HCV-infected patients (1, 2, 9) and that HCV-associated apoptosis involves, at least partly, a mitochondrion-mediated pathway (2). In those clinical settings, however, it is not clear whether apoptosis is mediated by host immune responses through the activity of cytotoxic T lymphocytes or whether it is mediated directly by HCV replication and/or protein expression itself. In experimental settings, ectopic expression of HCV core (13, 36), E2 (12), and NS4A (43) has been shown to induce mitochondrion-mediated apoptosis in cultured cells. However, these observations need to be verified in the context of virus replication. The recent development of an efficient HCV infection system in cell culture (37, 66, 71) has allowed us to investigate whether HCV replication directly causes apoptosis. In the present study, we have demonstrated that HCV infection induces Bax-triggered, mitochondrion-mediated, caspase 3-dependent apoptosis, as evidenced by increased accumulation of Bax on mitochondria and its conformational change (Fig. 3), decreased mitochondrial transmembrane potential (Fig. 4), and mitochondrial swelling (Fig. 5), which lead to the release of cytochrome *c* from the mitochondria (Fig. 6A) and subsequent activation of caspase 9 and caspase 3 (Fig. 6B and 2, respectively).

We also observed increased production of mitochondrial superoxide in HCV-infected cells (Fig. 7). This result is consistent with previous observations that expression of the entire HCV polyprotein (47) or HCV replication (60) enhanced production of ROS, including superoxide, through deregulation of mitochondrial calcium homeostasis. ROS, which are produced through the mitochondrial respiratory chain (8), were reported to trigger conformational change, dimerization, and mitochondrial translocation of Bax (18, 42). It is likely, therefore, that activation of Bax in HCV-infected cells is mediated, at least partly, through increased production of ROS in the mitochondria. Kim et al. (29) reported that ROS is a potent activator of c-Jun N-terminal protein kinase, which can phosphorylate Bax, leading to its activation and mitochondrial translocation. In

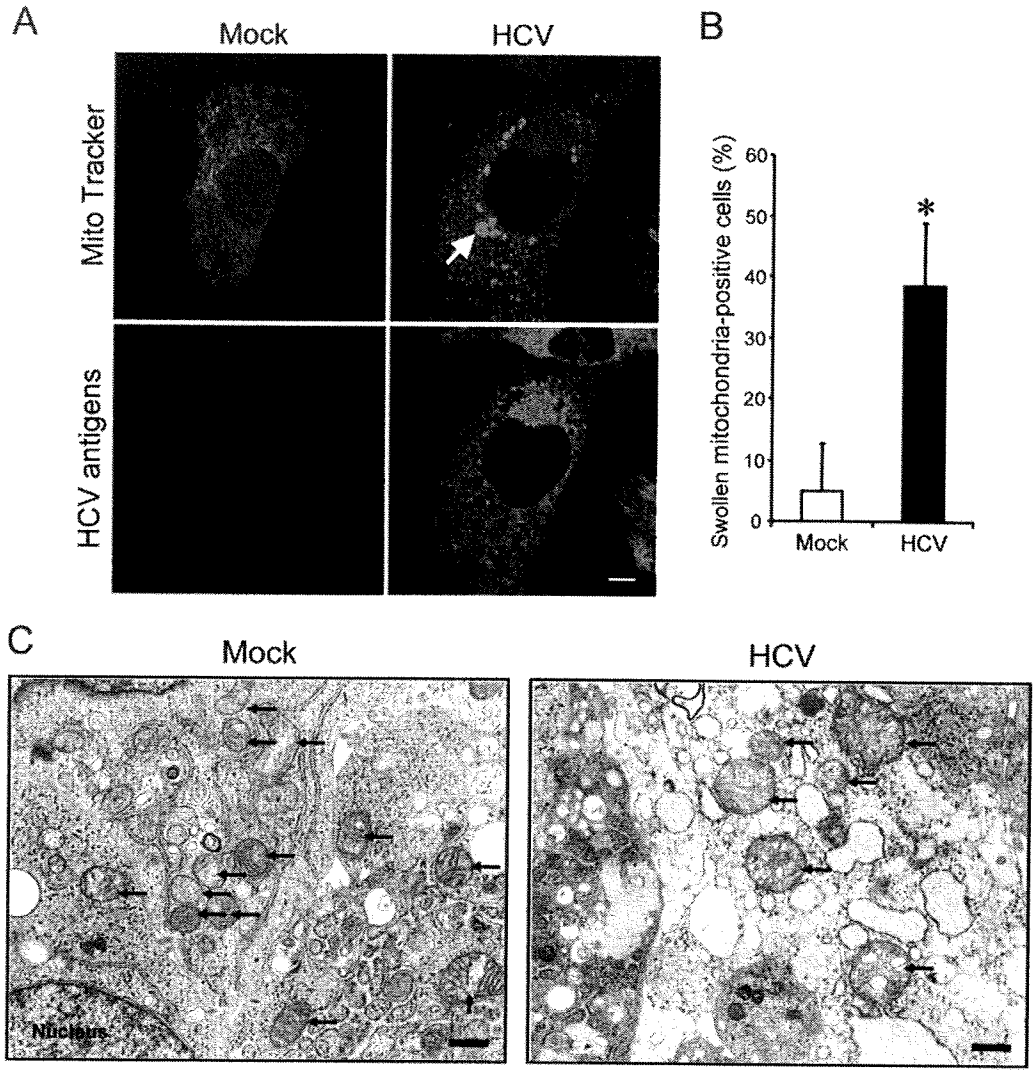

FIG. 5. HCV infection induces mitochondrial morphology changes in Huh7.5 cells. (A) Fluorescence microscopy analysis. Mitochondrial morphologies of HCV-infected cells and the mock-infected control at 6 days postinfection were examined by confocal microscopy. The cells were directly incubated with MitoTracker (upper row) and then stained for HCV antigens by using an HCV-infected patient's serum, followed by FITC-labeled goat anti-human IgG (bottom row). Scale bar, 5 μm. (B) Quantification of swollen mitochondrion-positive cells. The percentages of cells exhibiting swollen and/or aggregated mitochondria were determined for HCV-infected cultures and the mock-infected control. Data represent means ± standard deviations of three independent experiments. *, $P < 0.01$, compared with the control. (C) Electron microscopic analysis. Mitochondrial morphologies of HCV-infected cells and the mock-infected control at 6 days postinfection were examined by electron microscopy. Arrows indicate mitochondria. Scale bar, 1 μm.

this connection, HCV core protein has been shown to play a role in generating mitochondrial ROS (30). It was also reported that HCV core protein bound to the 14-3-3ε protein to dissociate Bax from the Bax/14-3-3ε complex, thereby promoting the Bax translocation to the mitochondria (36).

In addition to the caspase 9 activation that is mediated through the mitochondrial death (intrinsic) pathway, caspase 8 activation was seen in HCV-infected cells, though to a lesser extent (Fig. 6B and C). Caspase 8 is a key component of the extrinsic death pathway initiated by the TNF family members (31, 62). This pathway involves death receptors, such as Fas, TNF receptor, and TNF-related apoptosis-inducing ligand (TRAIL) receptors, which transduce signals to induce apoptosis upon binding to their respective ligands (52). In HCV-infected patients, the Fas-mediated signal pathway is involved in apoptosis of virus-infected hepatocytes (24). It was also reported that HCV (JFH1 strain) infection induced apoptosis through a TRAIL-mediated pathway in LH86 cells (72). On the other hand, a caspase 9-mediated activation of caspase 8, which is considered a cross talk between the intrinsic and the extrinsic death pathways, in certain cell systems was also reported (10, 11, 65). Whether the observed caspase 8 activation in HCV-infected cells was mediated through the extrinsic death pathway initiated by a cytokine(s) produced in the culture or whether it was mediated through the cross talk between the intrinsic and the extrinsic death pathways awaits further investigation. In this connection, activated caspase 8 is known to cleave the proapoptotic protein Bid to generate the Bid

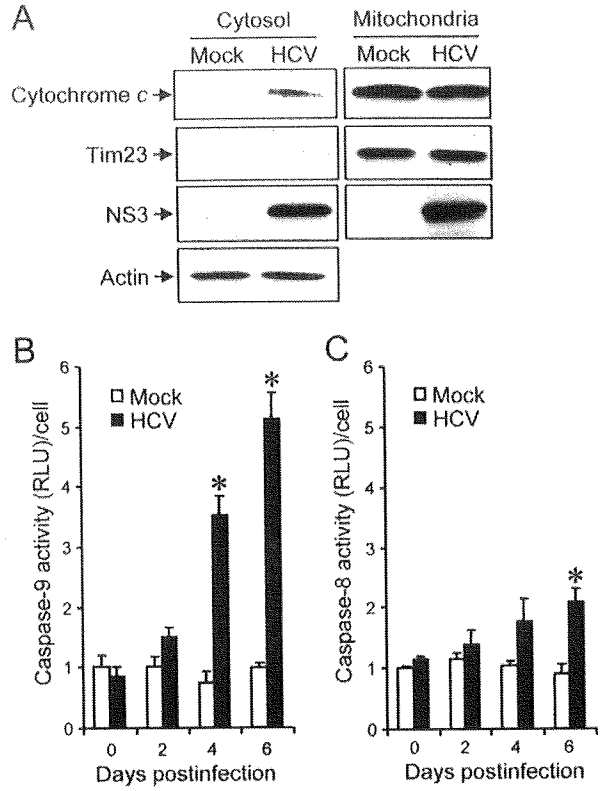

FIG. 6. HCV infection induces cytochrome *c* release and caspase 9 activation in Huh7.5 cells. (A) Cytochrome *c* release. Mitochondrial and cytosolic fractions were prepared from HCV-infected cells and the mock-infected control at 6 days postinfection and analyzed by immunoblotting using antibodies against cytochrome *c*, Tim23, NS3, and actin. Can Get Signal (Toyobo, Osaka, Japan) was used to obtain stronger signals for cytochrome *c*. Amounts of Tim23 and actin were measured to verify equal amounts of mitochondrial and cytosolic fractions, respectively. Also, Tim23 was used to show successful separation of mitochondria. (B) Caspase 9 activation. Caspase 9 activities in cells infected with HCV and mock-infected controls were measured at 0, 2, 4, and 6 days postinfection. The caspase 9 activity of the control cells at day 0 postinfection was arbitrarily expressed as 1.0. Data represent means ± standard deviations (SD) of three independent experiments. *, $P < 0.05$, compared with the control. (C) HCV infection induces a marginal degree of caspase 8 activation. Caspase 8 activities in cells infected with HCV and mock-infected controls were measured at 0, 2, 4, and 6 days postinfection. The caspase 8 activity of the control cells at day 0 postinfection was arbitrarily expressed as 1.0. Data represent means ± SD of three independent experiments. *, $P < 0.05$, compared with the control.

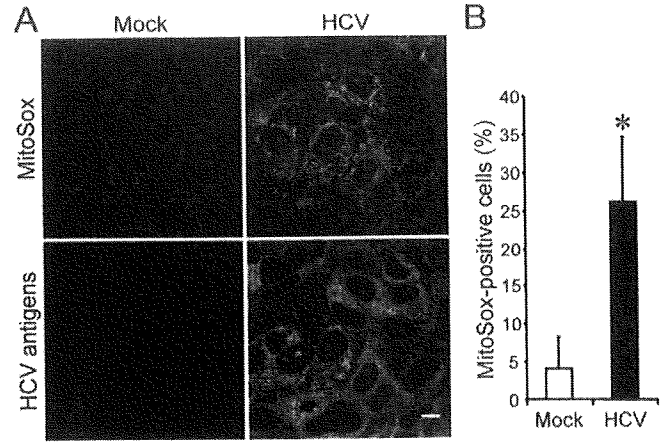

FIG. 7. HCV infection induces increased production of mitochondrial superoxide in Huh7.5 cells. (A) Mitochondrial superoxide production in HCV-infected cells and the mock-infected control was examined at 6 days postinfection. Cells were directly incubated with MitoSOX (upper row) and then stained for HCV antigens by using an HCV-infected patient's serum, followed by FITC-labeled goat anti-human IgG (bottom row). Scale bar, 10 μm. (B) Quantification of MitoSOX-stained cells. The percentages of cells stained with MitoSOX were determined for HCV-infected cultures and the mock-infected control. Data represent means ± standard deviations of three independent experiments. *, $P < 0.05$, compared with the control.

such as the accumulation of unfolded or misfolded proteins in the lumen. On the other hand, in response to ER stress, the unfolded protein response (UPR) is activated to alleviate the ER stress by stimulating protein folding and degradation in the ER as well as by inhibiting protein synthesis (7). The UPR of the host cell is disadvantageous for progeny virus production and may therefore be considered an antiviral host cell response. It was reported that, to counteract the disadvantageous UPR so as to maintain viral protein synthesis, HCV RNA replication suppressed the IRE1-XBP1 pathway, which is responsible for protein degradation upon UPR (59). Also, HCV E2 was shown to inhibit the double-stranded RNA-activated protein kinase-like ER-resident kinase (PERK), which attenuates protein synthesis during ER stress by phosphorylating the alpha subunit of eukaryotic translation initiation factor 2 (45). It is reasonable, therefore, to assume that HCV-infected cells may not necessarily exhibit typical responses to ER stress. In fact, our results revealed that HCV infection in Huh7.5 cells did not enhance

cleavage product truncated Bid (tBid), which facilitates the activation of Bax (63, 68). Under our experimental conditions, however, tBid was barely detected in HCV-infected cells even at 6 days postinfection (data not shown). It is thus likely that caspase 8 activation is marginal and is not the primary cause of Bax activation in our experimental system.

HCV protein expression and HCV RNA replication take place primarily in the ER or an ER-like membranous structure (39, 46). Like other members of the family *Flaviviridae*, such as dengue virus (69), Japanese encephalitis virus (69), West Nile virus (41), and bovine viral diarrhea virus (26), HCV has been reported to induce ER stress in the host cells (5, 14, 17, 55, 60). ER stress is triggered by perturbations in normal ER function,

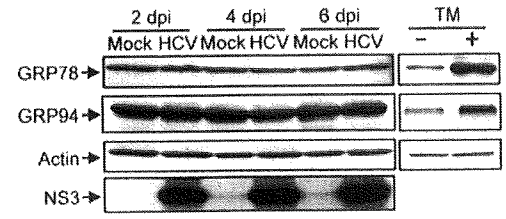

FIG. 8. HCV infection does not induce ER stress in Huh7.5 cells. Huh7.5 cells infected with HCV and mock-infected controls were harvested at 2, 4, and 6 days postinfection (dpi), and the whole-cell lysates were subjected to immunoblot analysis using antibodies against GRP78, GRP94, NS3, and actin. Amounts of actin were measured to verify equal amounts of sample loading. Huh7.5 cells treated with tunicamycin (TM; 5 μg/ml) for 48 h served as a positive control.

expression of GRP78 and GRP94, which are ER stress-induced chaperone proteins (Fig. 8). Our result thus implies the possibility that ER stress is not crucially involved in HCV-induced apoptosis in Huh7.5 cells. Taking advantage of this phenomenon, we could demonstrate that an ER stress-independent, mitochondrion-mediated pathway plays an important role in HCV-induced apoptosis. In this connection, Korenaga et al. (30) reported that HCV core protein increased ROS production in isolated mitochondria, independently of ER stress, by selectively inhibiting electron transport complex I activity.

In this study, we observed that increased ROS production, Bax activation, and caspase 3 activation were detectable in approximately 15% to 25% of HCV antigen-positive Huh7.5cells at 6 days postinfection (Fig. 7B, 3D, and 2D, respectively). On the other hand, >90% of the cells in the cultures were confirmed positive for HCV antigens (Fig. 1B). These results imply the possibility that HCV establishes persistent infection in Huh7.5 cells, with a minor fraction of virus-infected cells beginning to undergo apoptosis after a prolonged period of time. Alternatively, it is possible that Huh7.5 cells, though being derived from a cell line (6), are a mixture of two sublineages, with one sublineage being apoptosis prone and the other apoptosis resistant. To test the latter possibility, further cloning of Huh7.5 cells is now under way in our laboratory.

In conclusion, our present results collectively suggest that HCV infection induces apoptosis through a Bax-triggered, mitochondrion-mediated, caspase 3-dependent pathway.

ACKNOWLEDGMENTS

We are grateful to C. M. Rice (Center for the Study of Hepatitis C, The Rockefeller University) for providing pFL-J6/JFH1 and Huh7.5 cells.

This work was supported in part by grants-in-aid for scientific research from the Ministry of Education, Culture, Sports, Science and Technology (MEXT) and the Ministry of Health, Labor and Welfare, Japan.

This study was carried out as part of the Program of Founding Research Centers for Emerging and Reemerging Infectious Diseases, MEXT, Japan. This study was also part of the 21st Century Center of Excellence Program at Kobe University Graduate School of Medicine.

REFERENCES

1. **Bantel, H., A. Lügering, C. Poremba, N. Lügering, J. Held, W. Domschke, and K. Schulze-Osthoff.** 2001. Caspase activation correlates with the degree of inflammatory liver injury in chronic hepatitis C virus infection. Hepatology **34**:758–767.
2. **Bantel, H., and K. Schulze-Osthoff.** 2003. Apoptosis in hepatitis C virus infection. Cell Death Differ. **10**:S48–S58.
3. **Barbaro, G., G. Di Lorenzo, A. Asti, M. Ribersani, G. Belloni, B. Grisorio, G. Filice, and G. Barbarini.** 1999. Hepatocellular mitochondrial alterations in patients with chronic hepatitis C: ultrastructural and biochemical findings. Am. J. Gastroenterol. **94**:2198–2205.
4. **Bartenschlager, R., M. Frese, and T. Pietschmann.** 2004. Novel insights into hepatitis C virus replication and persistence. Adv. Virus Res. **63**:171–180.
5. **Benali-Furet, N. L., M. Chami, L. Houel, F. De Giorgi, F. Vernejoul, D. Lagorce, L. Buscail, R. Bartenschlager, F. Ichas, R. Rizzuto, and P. Paterlini-Bréchot.** 2005. Hepatitis C virus core triggers apoptosis in liver cells by inducing ER stress and ER calcium depletion. Oncogene **24**:4921–4933.
6. **Blight, K. J., J. A. McKeating, and C. M. Rice.** 2002. Highly permissive cell lines for subgenomic and genomic hepatitis C virus RNA replication. J. Virol. **76**:13001–13014.
7. **Boyce, M., and J. Yuan.** 2006. Cellular response to endoplasmic reticulum stress: a matter of life or death. Cell Death Differ. **13**:363–373.
8. **Brookes, P. S.** 2005. Mitochondrial H^+ leak and ROS generation: an odd couple. Free Radic. Biol. Med. **38**:12–23.
9. **Calabrese, F., P. Pontisso, E. Pettenazzo, L. Benvegnù, A. Vario, L. Chemello, A. Alberti, and M. Valente.** 2000. Liver cell apoptosis in chronic hepatitis C correlates with histological but not biochemical activity or serum HCV-RNA levels. Hepatology **31**:1153–1159.
10. **Camacho-Leal, P., and C. P. Stanners.** 2008. The human carcinoembryonic antigen (CEA) GPI anchor mediates anoikis inhibition by inactivation of the intrinsic death pathway. Oncogene **27**:1545–1553.
11. **Chae, Y. J., H. S. Kim, H. Rhim, B. E. Kim, S. W. Jeong, and I. K. Kim.** 2001. Activation of caspase-8 in 3-deazaadenosine-induced apoptosis of U-937 cells occurs downstream of caspase-3 and caspase-9 without Fas receptor-ligand interaction. Exp. Mol. Med. **4**:284–292.
12. **Chiou, H. L., Y. S. Hsieh, M. R. Hsieh, and T. Y. Chen.** 2006. HCV E2 may induce apoptosis of Huh-7 cells via a mitochondrial-related caspase pathway. Biochem. Biophys. Res. Commun. **345**:453–458.
13. **Chou, A. H., H. F. Tsai, Y. Y. Wu, C. Y. Hu, L. H. Hwang, P. I. Hsu, and P. N. Hsu.** 2005. Hepatitis C virus core protein modulates TRAIL-mediated apoptosis by enhancing Bid cleavage and activation of mitochondria apoptosis signaling pathway. J. Immunol. **174**:2160–2166.
14. **Christen, V., S. Treves, F. H. Duong, and M. H. Heim.** 2007. Activation of endoplasmic reticulum stress response by hepatitis viruses up-regulates protein phosphatase 2A. Hepatology **46**:558–565.
15. **Ciccaglione, A. R., C. Marcantonio, A. Costantino, M. Equestre, and M. Rapicetta.** 2003. Expression of HCV E1 protein in baculovirus-infected cells: effects on cell viability and apoptosis induction. Intervirology **46**:121–126.
16. **Ciccaglione, A. R., C. Marcantonio, E. Tritarelli, M. Equestre, F. Magurano, A. Costantino, L. Nicoletti, and M. Rapicetta.** 2004. The transmembrane domain of hepatitis C virus E1 glycoprotein induces cell death. Virus Res. **104**:1–9.
17. **Ciccaglione, A. R., C. Marcantonio, E. Tritarelli, M. Equestre, F. Vendittelli, A. Costantino, A. Geraci, and M. Rapicetta.** 2007. Activation of the ER stress gene gadd153 by hepatitis C virus sensitizes cells to oxidant injury. Virus Res. **126**:128–138.
18. **D'Alessio, M., M. De Nicola, S. Coppola, G. Gualandi, L. Pugliese, C. Cerella, S. Cristofanon, P. Civitareale, M. R. Ciriolo, A. Bergamaschi, A. Magrini, and L. Ghibelli.** 2005. Oxidative Bax dimerization promotes its translocation to mitochondria independently of apoptosis. FASEB J. **19**: 1504–1506.
19. **Egger, D., B. Wölk, R. Gosert, L. Bianchi, H. E. Blum, D. Moradpour, and K. Bienz.** 2002. Expression of hepatitis C virus proteins induces distinct membrane alterations including a candidate viral replication complex. J. Virol. **76**:5974–5984.
20. **Elbein, A. D.** 1987. Inhibitors of the biosynthesis and processing of N-linked oligosaccharide chains. Annu. Rev. Biochem. **56**:497–534.
21. **Erdtmann, L., N. Franck, H. Lerat, J. Le Seyec, D. Gilot, I. Cannie, P. Gripon, U. Hibner, and C. Guguen-Guillouzo.** 2003. The hepatitis C virus NS2 protein is an inhibitor of CIDE-B-induced apoptosis. J. Biol. Chem. **278**:18256–18264.
22. **Griffin, S., D. Clarke, C. McCormick, D. Rowlands, and M. Harris.** 2005. Signal peptide cleavage and internal targeting signals direct the hepatitis C virus p7 protein to distinct intracellular membranes. J. Virol. **79**:15525–15536.
23. **Hidajat, R., M. Nagano-Fujii, L. Deng, M. Tanaka, Y. Takigawa, S. Kitazawa, and H. Hotta.** 2005. Hepatitis C virus NS3 protein interacts with ELKS-δ and ELKS-α, members of a novel protein family involved in intracellular transport and secretory pathways. J. Gen. Virol. **86**:2197–2208.
24. **Jarmay, K., G. Karacsony, Z. Ozsvar, I. Nagy, J. Lonovics, and Z. Schaff.** 2002. Assessment of histological feature in chronic hepatitis C. Hepatogastroenterology **49**:239–243.
25. **Jiang, C. C., L. H. Chen, S. Gillespie, K. A. Kiejda, N. Mhaidat, Y. F. Wang, R. Thorne, X. D. Zhang, and P. Hersey.** 2007. Tunicamycin sensitizes human melanoma cells to tumor necrosis factor-related apoptosis-inducing ligand-induced apoptosis by up-regulation of TRAIL-R2 via the unfolded protein response. Cancer Res. **67**:5880–5888.
26. **Jordan, R., L. Wang, T. M. Graczyk, T. M. Block, and P. R. Romano.** 2002. Replication of a cytopathic strain of bovine viral diarrhea virus activates PERK and induces endoplasmic reticulum stress-mediated apoptosis of MDBK cells. J. Virol. **76**:9588–9599.
27. **Kaasik, A., D. Safiulina, A. Zharkovsky, and V. Veksler.** 2007. Regulation of mitochondrial matrix volume. Am. J. Physiol. Cell Physiol. **292**:C157–C163.
28. **Kamada, S., U. Kikkawa, Y. Tsujimoto, and T. Hunter.** 2005. Nuclear translocation of caspase-3 is dependent on its proteolytic activation and recognition of a substrate-like protein(s). J. Biol. Chem. **280**:857–860.
29. **Kim, B. J., S. W. Ryu, and B. J. Song.** 2006. JNK- and p38 kinase-mediated phosphorylation of Bax leads to its activation and mitochondrial translocation and to apoptosis of human hepatoma HepG2 cells. J. Biol. Chem. **281**:21256–21265.
30. **Korenaga, M., T. Wang, Y. Li, L. A. Showalter, T. Chan, J. Sun, and S. A. Weinman.** 2005. Hepatitis C virus core protein inhibits mitochondrial electron transport and increases reactive oxygen species (ROS) production. J. Biol. Chem. **280**:37481–37488.
31. **Kumar, S.** 2007. Caspase function in programmed cell death. Cell Death Differ. **14**:32–43.
32. **Lalier, L., P. F. Cartron, P. Juin, S. Nedelkina, S. Manon, B. Bechinger, and**

F. M. Vallette. 2007. Bax activation and mitochondrial insertion during apoptosis. Apoptosis 12:887–896.
33. Lan, K. H., M. L. Sheu, S. J. Hwang, S. H. Yen, S. Y. Chen, J. C. Wu, Y. J. Wang, N. Kato, M. Omata, F. Y. Chang, and S. D. Lee. 2002. HCV NS5A interacts with p53 and inhibits p53-mediated apoptosis. Oncogene 21:4801–4811.
34. Lee, A. S. 2001. The glucose-regulated proteins: stress induction and clinical applications. Trends Biochem. Sci. 26:504–510.
35. Lee, S. H., Y. K. Kim, C. S. Kim, S. K. Seol, J. Kim, S. Cho, Y. L. Song, R. Bartenschlager, and S. K. Jang. 2005. E2 of hepatitis C virus inhibits apoptosis. J. Immunol. 175:8226–8235.
36. Lee, S. K., S. O. Park, C. O. Joe, and Y. S. Kim. 2007. Interaction of HCV core protein with 14-3-3ε protein releases Bax to activate apoptosis. Biochem. Biophys. Res. Commun. 352:756–762.
37. Lindenbach, B. D., M. J. Evans, A. J. Syder, B. Wölk, T. L. Tellinghuisen, C. C. Liu, T. Maruyama, R. O. Hynes, D. R. Burton, J. A. McKeating, and C. M. Rice. 2005. Complete replication of hepatitis C virus in cell culture. Science 309:623–626.
38. Lindenbach, B. D., P. Meuleman, A. Ploss, T. Vanwolleghem, A. J. Syder, J. A. McKeating, R. E. Lanford, S. M. Feinstone, M. E. Major, G. Leroux-Roels, and C. M. Rice. 2006. Cell culture-grown hepatitis C virus is infectious in vivo and can be recultured in vitro. Proc. Natl. Acad. Sci. USA 103:3805–3809.
39. Lindenbach, B. D., and C. M. Rice. 2005. Unravelling hepatitis C virus replication from genome to function. Nature 436:933–938.
40. Marusawa, H., M. Hijikata, T. Chiba, and K. Shimotohno. 1999. Hepatitis C virus core protein inhibits Fas- and tumor necrosis factor alpha-mediated apoptosis via NF-κB activation. J. Virol. 73:4713–4720.
41. Medigeshi, G. R., A. M. Lancaster, A. J. Hirsch, T. Briese, W. I. Lipkin, V. Defilippis, K. Früh, P. W. Mason, J. Nikolich-Zugich, and J. A. Nelson. 2007. West Nile virus infection activates the unfolded protein response, leading to CHOP induction and apoptosis. J. Virol. 81:10849–10860.
42. Nie, C., C. Tian, L. Zhao, P. X. Petit, M. Mehrpour, and Q. Chen. 2008. Cysteine 62 of Bax is critical for its conformational activation and its pro-apoptotic activity in response to H_2O_2-induced apoptosis. J. Biol. Chem. 283:15359–15369.
43. Nomura-Takigawa, Y., M. Nagano-Fujii, L. Deng, S. Kitazawa, S. Ishido, K. Sada, and H. Hotta. 2006. Non-structural protein 4A of Hepatitis C virus accumulates on mitochondria and renders the cells prone to undergoing mitochondria-mediated apoptosis. J. Gen. Virol. 87:1935–1945.
44. Oliver, F. J., G. de la Rubia, V. Rolli, M. C. Ruiz-Ruiz, G. de Murcia, and J. M. Murcia. 1998. Importance of poly(ADP-ribose) polymerase and its cleavage in apoptosis. J. Biol. Chem. 273:33533–33539.
45. Pavio, N., P. R. Romano, T. M. Graczyk, S. M. Feinstone, and D. R. Taylor. 2003. Protein synthesis and endoplasmic reticulum stress can be modulated by the hepatitis C virus envelope protein E2 through the eukaryotic initiation factor 2α kinase PERK. J. Virol. 77:3578–3585.
46. Pawlotsky, J. M., S. Chevaliez, and J. G. McHutchison. 2007. The hepatitis C virus life cycle as a target for new antiviral therapies. Gastroenterology. 132:1979–1998.
47. Piccoli, C., R. Scrima, G. Quarato, A. D'Aprile, M. Ripoli, L. Lecce, D. Boffoli, D. Moradpour, and N. Capitanio. 2007. Hepatitis C virus protein expression causes calcium-mediated mitochondrial bioenergetic dysfunction and nitro-oxidative stress. Hepatology 46:58–65.
48. Prikhod'ko, E. A., G. G. Prikhod'ko, R. M. Siegel, P. Thompson, M. E. Major, and J. I. Cohen. 2004. The NS3 protein of hepatitis C virus induces caspase-8-mediated apoptosis independent of its protease or helicase activities. Virology 329:53–67.
49. Ray, R. B., K. Meyer, R. Steele, A. Shrivastava, B. B. Aggarwal, and R. Ray. 1998. Inhibition of tumor necrosis factor (TNF-α)-mediated apoptosis by hepatitis C virus core protein. J. Biol. Chem. 273:2256–2259.
50. Safiulina, D., V. Veksler, A. Zharkovsky, and A. Kaasik. 2006. Loss of mitochondrial membrane potential is associated with increase in mitochondrial volume: physiological role in neurones. J. Cell. Physiol. 206:347–353.
51. Saito, K., K. Meyer, R. Warner, A. Basu, R. B. Ray, and R. Ray. 2006. Hepatitis C virus core protein inhibits tumor necrosis factor alpha-mediated apoptosis by a protective effect involving cellular FLICE inhibitory protein. J. Virol. 80:4372–4379.
52. Schulze-Osthoff, K., D. Ferrari, M. Los, S. Wesselborg, and M. E. Peter. 1998. Apoptosis signaling by death receptors. Eur. J. Biochem. 254:439–459.
53. Schwer, B., S. Ren, T. Pietschmann, J. Kartenbeck, K. Kaehlcke, R. Bartenschlager, T. S. Yen, and M. Ott. 2004. Targeting of hepatitis C virus core protein to mitochondria through a novel C-terminal localization motif. J. Virol. 78:7958–7968.
54. Scorrano, L., M. Ashiya, K. Buttle, S. Weiler, S. A. Oakes, C. A. Mannella, and S. J. Korsmeyer. 2002. A distinct pathway remodels mitochondrial cristae and mobilizes cytochrome c during apoptosis. Dev. Cell 2:55–67.
55. Sekine-Osajima, Y., N. Sakamoto, K. Mishima, M. Nakagawa, Y. Itsui, M. Tasaka, Y. Nishimura-Sakurai, C. H. Chen, T. Kanai, K. Tsuchiya, T. Wakita, N. Enomoto, and M. Watanabe. 2008. Development of plaque assays for hepatitis C virus-JFH1 strain and isolation of mutants with enhanced cytopathogenicity and replication capacity. Virology 371:71–85.
56. Shepard, C. W., L. Finelli, and M. J. Alter. 2005. Global epidemiology of hepatitis C virus infection. Lancet Infect. Dis. 5:558–567.
57. Siavoshian, S., J. D. Abraham, C. Thumann, M. P. Kieny, and C. Schuster. 2005. Hepatitis C virus core, NS3, NS5A, NS5B proteins induce apoptosis in mature dendritic cells. J. Med. Virol. 75:402–411.
58. Tanaka, M., M. Nagano-Fujii, L. Deng, S. Ishido, K. Sada, and H. Hotta. 2006. Single-point mutations of hepatitis C virus that impair p53 interaction and anti-apoptotic activity of NS3. Biochem. Biophys. Res. Commun. 340:792–799.
59. Tardif, K. D., K. Mori, R. J. Kaufman, and A. Siddiqui. 2004. Hepatitis C virus suppresses the IRE1-XBP1 pathway of the unfolded protein response. J. Biol. Chem. 279:17158–17164.
60. Tardif, K. D., G. Waris, and A. Siddiqui. 2005. Hepatitis C virus, ER stress, and oxidative stress. Trends Microbiol. 13:159–163.
61. Tewari, M., L. T. Quan, K. O'Rourke, S. Desnoyers, Z. Zeng, D. R. Beidler, G. G. Poirier, G. S. Salvesen, and V. M. Dixit. 1995. Yama/CPP32 beta, a mammalian homolog of CED-3, is a CrmA-inhibitable protease that cleaves the death substrate poly (ADP-ribose) polymerase. Cell 81:801–809.
62. Thorburn, A. 2004. Death receptor-induced cell killing. Cell. Signal. 16:139–144.
63. Tsujimoto, Y. 2003. Cell death regulation by the Bcl-2 protein family in the mitochondria. J. Cell. Physiol. 195:158–167.
64. Upton, J. P., A. J. Valentijn, L. Zhang, and A. P. Gilmore. 2007. The N-terminal conformation of Bax regulates cell commitment to apoptosis. Cell Death Differ. 14:932–942.
65. Viswanath, V., Y. Wu, R. Boonplueang, S. Chen, F. F. Stevenson, F. Yantiri, L. Yang, M. F. Beal, and J. K. Andersen. 2001. Caspase-9 activation results in downstream caspase-8 activation and bid cleavage in 1-methyl-4-phenyl-1,2,3,6-tetrahydropyridine-induced Parkinson's disease. J. Neurosci. 21:9519–9528.
66. Wakita, T., T. Pietschmann, T. Kato, T. Date, M. Miyamoto, Z. Zhao, K. Murthy, A. Habermann, H. G. Kräusslich, M. Mizokami, R. Bartenschlager, and T. J. Liang. 2005. Production of infectious hepatitis C virus in tissue culture from a cloned viral genome. Nat. Med. 11:791–796.
67. Wang, J., W. Tong, X. Zhang, L. Chen, Z. Yi, T. Pan, Y. Hu, L. Xiang, and Z. Yuan. 2006. Hepatitis C virus non-structural protein NS5A interacts with FKBP38 and inhibits apoptosis in Huh7 hepatoma cells. FEBS Lett. 580:4392–4400.
68. Wei, M. C., W. X. Zong, E. H. Cheng, T. Lindsten, V. Panoutsakopoulou, A. J. Ross, K. A. Roth, G. R. MacGregor, C. B. Thompson, and S. J. Korsmeyer. 2001. Proapoptotic BAX and BAK: a requisite gateway to mitochondrial dysfunction and death. Science 292:727–730.
69. Yu, C. Y., Y. W. Hsu, C. L. Liao, and Y. L. Lin. 2006. Flavivirus infection activates the XBP1 pathway of the unfolded protein response to cope with endoplasmic reticulum stress. J. Virol. 80:11868–11880.
70. Zhivotovsky, B., A. Samali, A. Gahm, and S. Orrenius. 1999. Caspases: their intracellular localization and translocation during apoptosis. Cell Death Differ. 6:644–651.
71. Zhong, J., P. Gastaminza, G. Cheng, S. Kapadia, T. Kato, D. R. Burton, S. F. Wieland, S. L. Uprichard, T. Wakita, and F. V. Chisari. 2005. Robust hepatitis C virus infection in vitro. Proc. Natl. Acad. Sci. USA 102:9294–9299.
72. Zhu, H., H. Dong, E. Eksioglu, A. Hemming, M. Cao, J. M. Crawford, D. R. Nelson, and C. Liu. 2007. Hepatitis C virus triggers apoptosis of a newly developed hepatoma cell line through antiviral defense system. Gastroenterology 133:1649–1659.
73. Zhu, N., A. Khoshnan, R. Schneider, M. Matsumoto, G. Dennert, C. Ware, and M. M. C. Lai. 1998. Hepatitis C virus core protein binds to the cytoplasmic domain of tumor necrosis factor (TNF) receptor 1 and enhances TNF-induced apoptosis. J. Virol. 72:3691–3697.

JOURNAL OF VIROLOGY, Mar. 2009, p. 2389–2392
0022-538X/09/$08.00+0 doi:10.1128/JVI.01690-08

Vol. 83, No. 5

Proteasomal Turnover of Hepatitis C Virus Core Protein Is Regulated by Two Distinct Mechanisms: a Ubiquitin-Dependent Mechanism and a Ubiquitin-Independent but PA28γ-Dependent Mechanism▽

Ryosuke Suzuki,[1] Kohji Moriishi,[2] Kouichirou Fukuda,[1] Masayuki Shirakura,[1] Koji Ishii,[1] Ikuo Shoji,[3] Takaji Wakita,[1] Tatsuo Miyamura,[1] Yoshiharu Matsuura,[2] and Tetsuro Suzuki[1]*

Department of Virology II, National Institute of Infectious Diseases, Tokyo 162-8640,[1] Department of Molecular Virology, Research Institute for Microbial Diseases, Osaka University, Osaka 565-0871,[2] and Division of Microbiology, Kobe University Graduate School of Medicine, Hyogo 650-0017,[3] Japan

Received 8 August 2008/Accepted 5 December 2008

We have previously reported on the ubiquitylation and degradation of hepatitis C virus core protein. Here we demonstrate that proteasomal degradation of the core protein is mediated by two distinct mechanisms. One leads to polyubiquitylation, in which lysine residues in the N-terminal region are preferential ubiquitylation sites. The other is independent of the presence of ubiquitin. Gain- and loss-of-function analyses using lysineless mutants substantiate the hypothesis that the proteasome activator PA28γ, a binding partner of the core, is involved in the ubiquitin-independent degradation of the core protein. Our results suggest that turnover of this multifunctional viral protein can be tightly controlled via dual ubiquitin-dependent and -independent proteasomal pathways.

Hepatitis C virus (HCV) core protein, whose amino acid sequence is highly conserved among different HCV strains, not only is involved in the formation of the HCV virion but also has a number of regulatory functions, including modulation of signaling pathways, cellular and viral gene expression, cell transformation, apoptosis, and lipid metabolism (reviewed in references 9 and 15). We have previously reported that the E6AP E3 ubiquitin (Ub) ligase binds to the core protein and plays an important role in polyubiquitylation and proteasomal degradation of the core protein (22). Another study from our group identified the proteasome activator PA28γ/REG-γ as an HCV core-binding partner, demonstrating degradation of the core protein via a PA28γ-dependent pathway (16, 17). In this work, we further investigated the molecular mechanisms underlying proteasomal degradation of the core protein and found that in addition to regulation by the Ub-mediated pathway, the turnover of the core protein is also regulated by PA28γ in a Ub-independent manner.

Although ubiquitylation of substrates generally requires at least one Lys residue to serve as a Ub acceptor site (5), there is no consensus as to the specificity of the Lys targeted by Ub (4, 8). To determine the sites of Ub conjugation in the core protein, we used site-directed mutagenesis to replace individual Lys residues or clusters of Lys residues with Arg residues in the N-terminal 152 amino acids (aa) of the core (C152), within which is contained all seven Lys residues (Fig. 1A). Plasmids expressing a variety of mutated core proteins were generated by PCR and inserted into the pCAGGS (18). Each core-expressing construct was transfected into human embryonic kidney 293T cells along with the pMT107 (25) encoding a Ub moiety tagged with six His residues (His_6). Transfected cells were treated with the proteasome inhibitor MG132 for 14 h to maximize the level of Ub-conjugated core intermediates by blocking the proteasome pathway and were harvested 48 h posttransfection. His_6-tagged proteins were purified from the extracts by Ni^{2+}-chelation chromatography. Eluted protein and whole lysates of transfected cells before purification were analyzed by Western blotting using anticore antibodies (Fig. 1B). Mutations replacing one or two Lys residues with Arg in the core protein did not affect the efficiency of ubiquitylation: detection of multiple Ub-conjugated core intermediates was observed in the mutant core proteins comparable to the results seen with the wild-type core protein as previously reported (23). In contrast, a substitution of four N-terminal Lys residues (C152K6-23R) caused a significant reduction in ubiquitylation (Fig. 1B, lane 9). Multiple Ub-conjugated core intermediates were not detected in the Lys-less mutant (C152KR), in which all seven Lys residues were replaced with Arg (Fig. 1B, lane 11). These results suggest that there is not a particular Lys residue in the core protein to act as the Ub acceptor but that more than one Lys located in its N-terminal region can serve as the preferential ubiquitylation site. In rare cases, Ub is known to be conjugated to the N terminus of proteins; however, these results indicate that this does not occur within the core protein.

To investigate how polyubiquitylation correlates with proteasome degradation of the core protein, we performed kinetic analysis of the wild-type and mutated core proteins by use of the Ub protein reference (UPR) technique, which can compensate for data scatter of sample-to-sample variations such as levels of expression (10, 24). Fusion proteins expressed from UPR-based constructs (Fig. 2A) were cotranslationally cleaved by deubiquitylating enzymes, thereby generating equimolar quantities of the core proteins and the reference protein, dihydrofolate reductase-hemagglutinin (DHFR-HA) tag-modified Ub, in which the Lys at aa 48 was replaced by Arg to prevent its polyubiquitylation (Ub^{R48}). After 24 h of transfec-

* Corresponding author. Mailing address: Department of Virology II, National Institute of Infectious Diseases, 1-23-1 Toyama, Shinjuku-ku, Tokyo 162-8640, Japan. Phone: 81-3-5285-1111. Fax: 81-3-5285-1161. E-mail: tesuzuki@nih.go.jp.

▽ Published ahead of print on 17 December 2008.

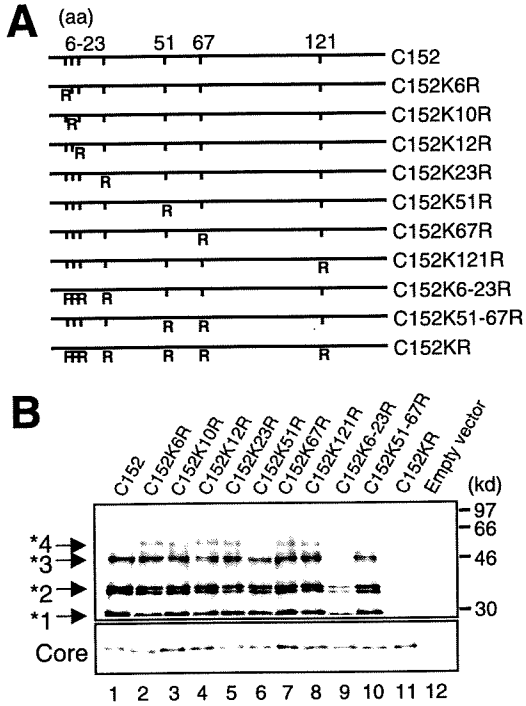

FIG. 1. In vivo ubiquitylation of HCV core protein. (A) The HCV core protein (N-terminal 152 aa) is represented on the top. The positions of the amino acid residues of the core protein are indicated above the bold lines. The positions of the seven Lys residues in the core are marked by vertical ticks. Substitution of Lys with Arg (R) is schematically depicted. (B) Detection of ubiquitylated forms of the core proteins. The transfected cells with core expression plasmids and pMT107 were treated with the proteasome inhibitor MG132 and harvested 48 h after transfection. His_6-tagged proteins were purified and subsequently analyzed by Western blot analysis using anticore antibody (upper panel). Core proteins conjugated to a number of His_6-Ub are denoted with asterisks. Whole lysates of transfected cells before purification were also analyzed (lower panel). Lanes 1 to 11, C152 to C152KR, as indicated for panel A. Lane 12; empty vector.

tion with UPR constructs, cells were treated with cycloheximide and the amounts of core proteins and DHFR-HA-Ub^{R48} at the indicated time points were determined by Western blot analysis using anticore and anti-HA antibodies. The mature form of the core protein, aa 1 to 173 (C173) (13, 20), and C152 were degraded with first-order kinetics (Fig. 2B and D). MG132 completely blocked the degradation of C173 and C152 (Fig. 2B), and C152K6-23R and C152KR were markedly stabilized (Fig. 2C). The half-lives of C173 and C152 were calculated to be 5 to 6 h, whereas those of C152K6-23R and C152KR were calculated to be 22 to 24 h (Fig. 2D), confirming that the Ub plays an important role in regulating degradation of the core protein. Nevertheless, these results also suggest possible involvement of the Ub-independent pathway in the turnover of the core protein, as C152KR is more destabilized than the reference protein (Fig. 2C and 2D).

We have shown that PA28γ specifically binds to the core protein and is involved in its degradation (16, 17). Recent studies demonstrated that PA28γ is responsible for Ub-independent degradation of the steroid receptor coactivator SRC-3 and cell cycle inhibitors such as p21 (3, 11, 12). Thus, we next investigated the possibility of PA28γ involvement in the deg-

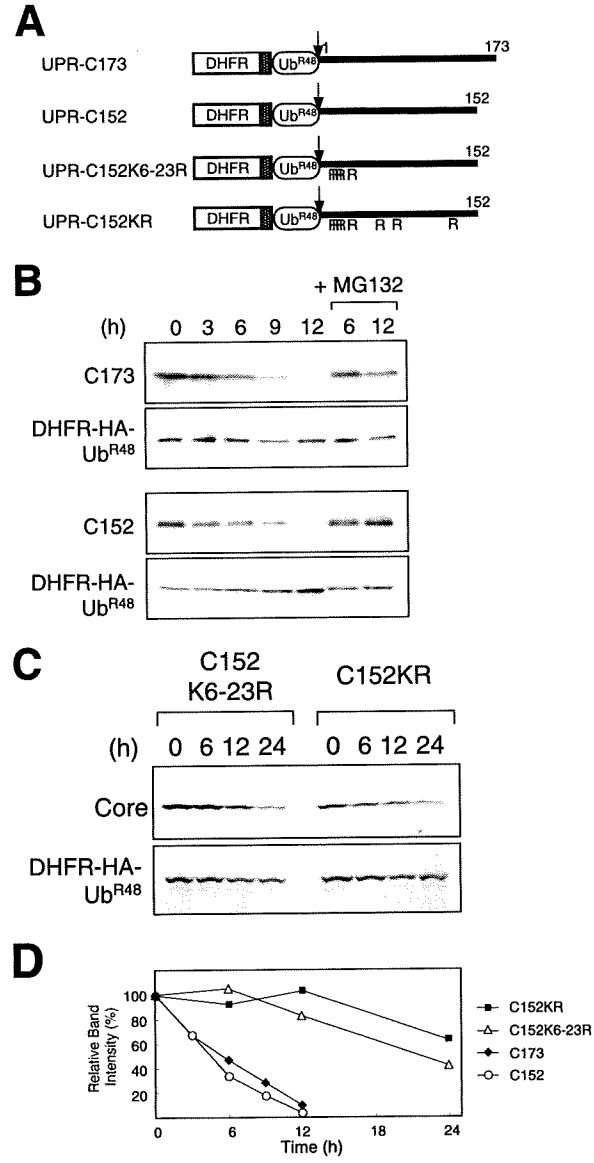

FIG. 2. Kinetic analysis of degradation of HCV core proteins. (A) The fusion constructs used in the UPR technique. Open boxes indicate the DHFR sequence, which is extended at the C terminus by a sequence containing the HA epitope (hatched boxes). Ub^{R48} moieties bearing the Lys-Arg substitution at aa 48 are represented by open ellipses. Bold lines indicate the regions of the core protein. The amino acid positions of the core protein are indicated above the bold lines. The arrows indicate the sites of in vivo cleavage by deubiquitylating enzymes. (B and C) Turnover of the core proteins. After a 24-h transfection with each UPR construct, cells were treated with 50 μg of cycloheximide/ml in the presence or absence of 10 μM MG132 for the different time periods indicated. Cells were lysed at the different time points indicated, followed by evaluation via sodium dodecyl sulfate-polyacrylamide gel electrophoresis and Western blot analysis using antibodies against the core protein and HA. (D) Quantitation of the data shown in panels B and C. At each time point, the ratio of band intensity of the core protein relative to the reference DHFR-HA-Ub^{R48} was determined by densitometry and is plotted as a percentage of the ratio at time zero.

radation of either C152KR or C152. Since C152KR carries two amino acid substitutions in the PA28γ-binding region (aa 44 to 71) (17), we tested the influence of the mutations of C152KR on the interaction with PA28γ by use of a coimmunoprecipi-

tation assay. When Flag-tagged PA28γ (F-PA28γ) was expressed in cells along with C152 or C152KR, F-PA28γ precipitated along with both C152 and C152KR, indicating that PA28γ interacts with both core proteins (Fig. 3A). Figure 3B reveals the effect of exogenous expression of F-PA28γ on the steady-state levels of C152 and C152KR. Consistent with previous data (17), the expression level of C152 was decreased to a nearly undetectable level in the presence of PA28γ (Fig. 3B, lanes 1 and 3). Interestingly, exogenous expression of PA28γ led to a marked reduction in the amount of C152KR expressed (Fig. 3B, lanes 5 and 7). Treatment with MG132 increased the steady-state level of the C152KR in the presence of F-PA28γ as well as the level of C152 (Fig. 3B, lanes 4 and 8).

We further investigated whether PA28γ affects the turnover of Lys-less core protein through time course experiments. C152KR was rapidly destabilized and almost completely degraded in a 3-h chase experiment using cells overexpressing F-PA28γ (Fig. 3C, left panels). A similar result was obtained using an analogous Lys-less mutant of the full-length core protein C191KR (Fig. 3C, right panels), thus demonstrating that the Lys-less core protein undergoes proteasomal degradation in a PA28γ-dependent manner. These results suggest that PA28γ may play a role in accelerating the turnover of the HCV core protein that is independent of ubiquitylation.

Finally, we examined gain- and loss-of-function of PA28γ with respect to degradation of full-length wild-type (C191) and mutated (C191KR) core proteins in human hepatoma Huh-7 cells. As expected, exogenous expression of PA28γ or E6AP caused a decrease in the C191 steady-state levels (Fig. 4A). In contrast, the C191KR level was decreased with expression of PA28γ but not of E6AP. We further used RNA interference to inhibit expression of PA28γ or E6AP. An increase in the abundance of C191KR was observed with PA28γ small interfering RNA (siRNA) but not with E6AP siRNA (Fig. 4B). An increase in the C191 level caused by the activity of siRNA against PA28γ or E6AP was confirmed as well.

Taking these results together, we conclude that turnover of the core protein is regulated by both Ub-dependent and Ub-independent pathways and that PA28γ is possibly involved in Ub-independent proteasomal degradation of the core protein. PA28 is known to specifically bind and activate the 20S proteasome (19). Thus, PA28γ may function by facilitating the delivery of the core protein to the proteasome in a Ub-independent manner.

Accumulating evidence suggests the existence of proteasome-dependent but Ub-independent pathways for protein degradation, and several important molecules, such as p53, p73, Rb, SRC-3, and the hepatitis B virus X protein, have two distinct degradation pathways that function in a Ub-dependent and Ub-independent manner (1, 2, 6, 7, 14, 21, 27). Recently, critical roles for PA28γ in the Ub-independent pathway have been demonstrated; SRC-3 and p21 can be recognized by the 20S proteasome independently of ubiquitylation through their interaction with PA28γ (3, 11, 12). It has also been reported that phosphorylation-dependent ubiquitylation mediated by GSK3 and SCF is important for SRC-3 turnover (26). Nevertheless, the precise mechanisms underlying turnover of most of the proteasome substrates that are regulated in both Ub-dependent and Ub-independent manners are not well understood. To our knowledge, the HCV core protein is the first

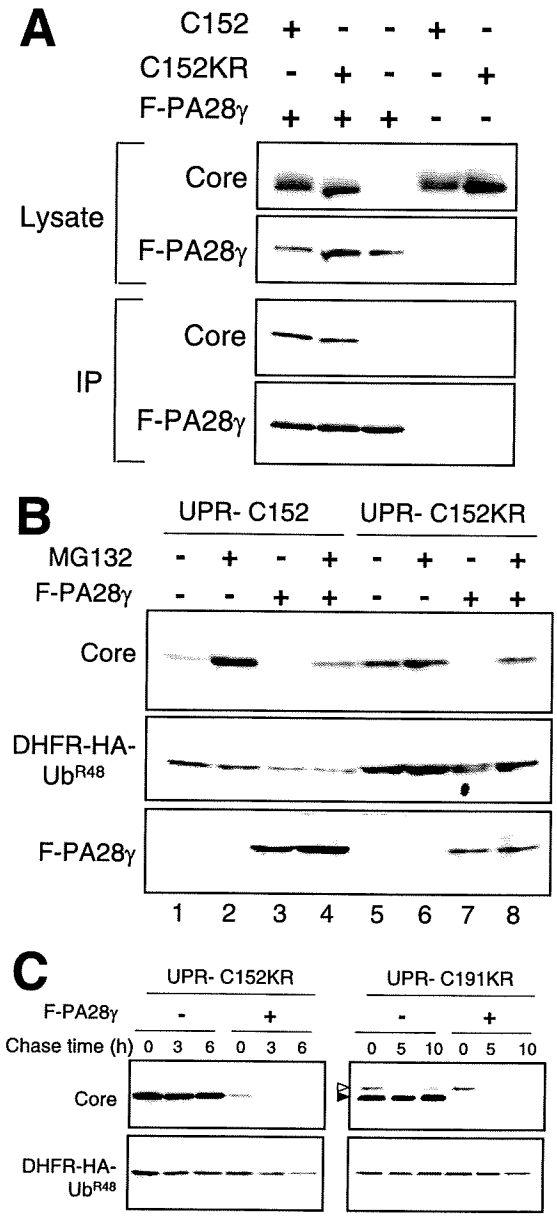

FIG. 3. PA28γ-dependent degradation of the core protein. (A) Interaction of the core protein with PA28γ. Cells were cotransfected with the wild-type (C152) or Lys-less (C152KR) core expression plasmid in the presence of a Flag-PA28γ (F-PA28γ) expression plasmid or an empty vector. The transfected cells were treated with MG132. After 48 h, the cell lysates were immunoprecipitated with anti-Flag antibody and visualized by Western blotting with anticore antibodies. Western blot analysis of whole cell lysates was also performed. (B) Degradation of the wild-type and Lys-less core proteins via the PA28γ-dependent pathway. Cells were transfected with the UPR construct with or without F-PA28γ. In some cases, cells were treated with 10 μM MG132 for 14 h before harvesting. Western blot analysis was performed using anticore, anti-HA, and anti-Flag antibodies. (C) After 24 h of transfection with UPR-C152KR and UPR-C191KR with or without F-PA28γ (an empty vector), cells were treated with 50 μg of cycloheximide/ml for different time periods as indicated (chase time). Western blot analysis was performed using anticore and anti-HA antibodies. The precursor core protein and the core that was processed, presumably by signal peptide peptidase, are denoted by open and closed triangles, respectively.

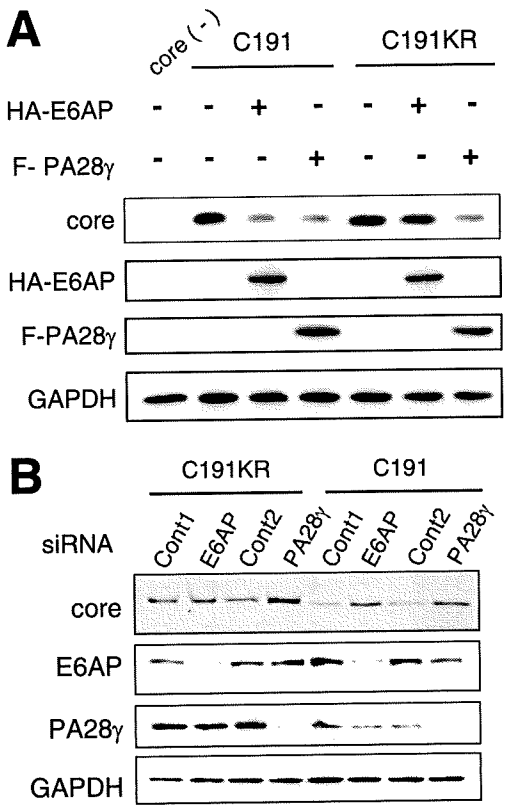

FIG. 4. Ub-dependent and Ub-independent degradation of the full-length core protein in hepatic cells. (A) Huh-7 cells were cotransfected with plasmids for the full-length core protein (C191) or its Lys-less mutant (C191KR) in the presence of F-PA28γ or HA-tagged-E6AP expression plasmid (HA-E6AP). After 48 h, cells were lysed and Western blot analysis was performed using anticore, anti-HA, anti-Flag, or anti-GAPDH. (B) Huh-7 cells were cotransfected with core expression plasmids along with siRNA against PA28γ or E6AP or with negative control siRNA. Cells were harvested 72 h after transfection and subjected to Western blot analysis.

viral protein studied that has led to identification of key cellular factors responsible for proteasomal degradation via dual distinct mechanisms. Although the question remains whether there is a physiological significance of the Ub-dependent and Ub-independent degradation of the core protein, it is reasonable to consider that tight control over cellular levels of the core protein, which is multifunctional and essential for viral replication, maturation, and pathogenesis, may play an important role in representing the potential for its functional activity.

This work was supported by a grant-in-aid for Scientific Research from the Japan Society for the Promotion of Science, from the Ministry of Health, Labor and Welfare of Japan, and from the Ministry of Education, Culture, Sports, Science and Technology, by Research on Health Sciences focusing on Drug Innovation from the Japan Health Sciences Foundation, Japan, and by the Program for Promotion of Fundamental Studies in Health Sciences of the National Institute of Biomedical Innovation of Japan.

REFERENCES

1. **Asher, G., J. Lotem, L. Sachs, C. Kahana, and Y. Shaul.** 2002. Mdm-2 and ubiquitin-independent p53 proteasomal degradation regulated by NQO1. Proc. Natl. Acad. Sci. USA **99:**13125–13130.
2. **Asher, G., P. Tsvetkov, C. Kahana, and Y. Shaul.** 2005. A mechanism of ubiquitin-independent proteasomal degradation of the tumor suppressors p53 and p73. Genes Dev. **19:**316–321.
3. **Chen, X., L. F. Barton, Y. Chi, B. E. Clurman, and J. M. Roberts.** 2007. Ubiquitin-independent degradation of cell-cycle inhibitors by the REGγ proteasome. Mol. Cell **26:**843–852.
4. **Ciechanover, A.** 1998. The ubiquitin-proteasome pathway: on protein death and cell life. EMBO J. **17:**7151–7160.
5. **Hershko, A., A. Ciechanover, and A. Varshavsky.** 2000. The ubiquitin system. Nat. Med. **6:**1073–1081.
6. **Jariel-Encontre, I., M. Pariat, F. Martin, S. Carillo, C. Salvat, and M. Piechaczyk.** 1995. Ubiquitinylation is not an absolute requirement for degradation of c-Jun protein by the 26 S proteasome. J. Biol. Chem. **270:**11623–11627.
7. **Jin, Y., H. Lee, S. X. Zeng, M. S. Dai, and H. Lu.** 2003. MDM2 promotes p21waf1/cip1 proteasomal turnover independently of ubiquitylation. EMBO J. **22:**6365–6377.
8. **Ju, D., and Y. Xie.** 2006. Identification of the preferential ubiquitination site and ubiquitin-dependent degradation signal of Rpn4. J. Biol. Chem. **281:**10657–10662.
9. **Lai, M. M. C., and C. F. Ware.** 1999. Hepatitis C virus core protein: possible roles in viral pathogenesis. Springer, Berlin, Germany.
10. **Lévy, F., N. Johnsson, T. Rumenapf, and A. Varshavsky.** 1996. Using ubiquitin to follow the metabolic fate of a protein. Proc. Natl. Acad. Sci. USA **93:**4907–4912.
11. **Li, X., L. Amazit, W. Long, D. M. Lonard, J. J. Monaco, and B. W. O'Malley.** 2007. Ubiquitin- and ATP-independent proteolytic turnover of p21 by the REGγ-proteasome pathway. Mol. Cell **26:**831–842.
12. **Li, X., D. M. Lonard, S. Y. Jung, A. Malovannaya, Q. Feng, J. Qin, S. Y. Tsai, M. J. Tsai, and B. W. O'Malley.** 2006. The SRC-3/AIB1 coactivator is degraded in a ubiquitin- and ATP-independent manner by the REGγ proteasome. Cell **124:**381–392.
13. **Liu, Q., C. Tackney, R. A. Bhat, A. M. Prince, and P. Zhang.** 1997. Regulated processing of hepatitis C virus core protein is linked to subcellular localization. J. Virol. **71:**657–662.
14. **Lonard, D. M., Z. Nawaz, C. L. Smith, and B. W. O'Malley.** 2000. The 26S proteasome is required for estrogen receptor-α and coactivator turnover and for efficient estrogen receptor-α transactivation. Mol. Cell **5:**939–948.
15. **Moradpour, D., F. Penin, and C. M. Rice.** 2007. Replication of hepatitis C virus. Nat. Rev. Microbiol. **5:**453–463.
16. **Moriishi, K., R. Mochizuki, K. Moriya, H. Miyamoto, Y. Mori, T. Abe, S. Murata, K. Tanaka, T. Miyamura, T. Suzuki, K. Koike, and Y. Matsuura.** 2007. Critical role of PA28γ in hepatitis C virus-associated steatogenesis and hepatocarcinogenesis. Proc. Natl. Acad. Sci. USA **104:**1661–1666.
17. **Moriishi, K., T. Okabayashi, K. Nakai, K. Moriya, K. Koike, S. Murata, T. Chiba, K. Tanaka, R. Suzuki, T. Suzuki, T. Miyamura, and Y. Matsuura.** 2003. Proteasome activator PA28γ-dependent nuclear retention and degradation of hepatitis C virus core protein. J. Virol. **77:**10237–10249.
18. **Niwa, H., K. Yamamura, and J. Miyazaki.** 1991. Efficient selection for high-expression transfectants with a novel eukaryotic vector. Gene **108:**193–199.
19. **Realini, C., C. C. Jensen, Z. Zhang, S. C. Johnston, J. R. Knowlton, C. P. Hill, and M. Rechsteiner.** 1997. Characterization of recombinant REGα, REGβ, and REGγ proteasome activators. J. Biol. Chem. **272:**25483–25492.
20. **Santolini, E., G. Migliaccio, and N. La Monica.** 1994. Biosynthesis and biochemical properties of the hepatitis C virus core protein. J. Virol. **68:**3631–3641.
21. **Sheaff, R. J., J. D. Singer, J. Swanger, M. Smitherman, J. M. Roberts, and B. E. Clurman.** 2000. Proteasomal turnover of p21Cip1 does not require p21Cip1 ubiquitination. Mol. Cell **5:**403–410.
22. **Shirakura, M., K. Murakami, T. Ichimura, R. Suzuki, T. Shimoji, K. Fukuda, K. Abe, S. Sato, M. Fukasawa, Y. Yamakawa, M. Nishijima, K. Moriishi, Y. Matsuura, T. Wakita, T. Suzuki, P. M. Howley, T. Miyamura, and I. Shoji.** 2007. E6AP ubiquitin ligase mediates ubiquitylation and degradation of hepatitis C virus core protein. J. Virol. **81:**1174–1185.
23. **Suzuki, R., K. Tamura, J. Li, K. Ishii, Y. Matsuura, T. Miyamura, and T. Suzuki.** 2001. Ubiquitin-mediated degradation of hepatitis C virus core protein is regulated by processing at its carboxyl terminus. Virology **280:**301–309.
24. **Suzuki, T., and A. Varshavsky.** 1999. Degradation signals in the lysine-asparagine sequence space. EMBO J. **18:**6017–6026.
25. **Treier, M., L. M. Staszewski, and D. Bohmann.** 1994. Ubiquitin-dependent c-Jun degradation in vivo is mediated by the δ domain. Cell **78:**787–798.
26. **Wu, R. C., Q. Feng, D. M. Lonard, and B. W. O'Malley.** 2007. SRC-3 coactivator functional lifetime is regulated by a phospho-dependent ubiquitin time clock. Cell **129:**1125–1140.
27. **Zhang, Z., and R. Zhang.** 2008. Proteasome activator PA28γ regulates p53 by enhancing its MDM2-mediated degradation. EMBO J. **27:**852–864.

ARTICLE

Journal of Cellular Biochemistry 106:1123-1135 (2009)

Identification of Annexin A1 as a Novel Substrate for E6AP-Mediated Ubiquitylation

Tetsu Shimoji,[1] Kyoko Murakami,[1] Yuichi Sugiyama,[1] Mami Matsuda,[1] Sachiko Inubushi,[2] Junichi Nasu,[1] Masayuki Shirakura,[1] Tetsuro Suzuki,[1] Takaji Wakita,[1] Tatsuya Kishino,[3] Hak Hotta,[2] Tatsuo Miyamura,[1] and Ikuo Shoji[1,2*]

[1]*Department of Virology II, National Institute of Infectious Diseases, Shinjuku-ku, Tokyo, Japan*

[2]*Division of Microbiology, Kobe University Graduate School of Medicine, Kobe, Hyogo, Japan*

[3]*Division of Functional Genomics, Center for Frontier Life Sciences, Nagasaki University, Nagasaki, Japan*

ABSTRACT

E6-associated protein (E6AP) is a cellular ubiquitin protein ligase that mediates ubiquitylation and degradation of p53 in conjunction with the high-risk human papillomavirus E6 proteins. However, the physiological functions of E6AP are poorly understood. To identify a novel biological function of E6AP, we screened for binding partners of E6AP using GST pull-down and mass spectrometry. Here we identified annexin A1, a member of the annexin superfamily, as an E6AP-binding protein. Ectopic expression of E6AP enhanced the degradation of annexin A1 in vivo. RNAi-mediated downregulation of endogenous E6AP increased the levels of endogenous annexin A1 protein. E6AP interacted with annexin A1 and induced its ubiquitylation in a Ca^{2+}-dependent manner. GST pull-down assay revealed that the annexin repeat domain III of annexin A1 is important for the E6AP binding. Taken together, our data suggest that annexin A1 is a novel substrate for E6AP-mediated ubiquitylation. Our findings raise the possibility that E6AP may play a role in controlling the diverse functions of annexin A1 through the ubiquitin-proteasome pathway. J. Cell. Biochem. 106: 1123–1135, 2009.

KEY WORDS: E6AP; ANNEXIN A1; UBIQUITIN; DEGRADATION

The ubiquitin/26S proteasome pathway plays important roles in the control of many basic cellular processes, such as cell cycle progression, signal transduction, transcriptional regulation, DNA repair, and the regulation of inflammation responses [Hershko and Ciechanover, 1998]. Ubiquitin is a 76-aa polypeptide that is highly conserved among eukaryotic organisms. The ubiquitin-proteasome pathway consists of an enzymatic cascade that ubiquitylates proteins, thereby targeting them for proteasomal degradation. The E1 ubiquitin-activating enzyme binds ubiquitin through a thioester linkage in an ATP-dependent manner [Ciechanover et al., 1981; Haas and Rose, 1982]. The activated ubiquitin is then transferred to the E2 ubiquitin-conjugating enzyme. E2 works in conjunction with the E3 ubiquitin-protein ligase, which is responsible for conferring substrate specificity [Hershko et al., 1986]. E3 mediates the transfer of ubiquitin to the target protein. The polyubiquitylated substrates are rapidly recognized and degraded by the 26S proteasome [Ciechanover, 1998; Ciechanover et al., 2000].

E6-associated protein (E6AP) was initially identified as the cellular factor that stimulates ubiquitin-dependent degradation of the tumor suppressor p53 in conjunction with the E6 protein of cervical cancer-associated human papillomavirus (HPV) types 16 and 18 [Huibregtse et al., 1993a; Scheffner et al., 1994]. The E6-E6AP complex functions as an E3 ubiquitin ligase in the ubiquitylation of p53 [Scheffner et al., 1993]. E6AP is the prototype of a family of ubiquitin ligases called HECT domain ubiquitin ligases, all of which contain a domain homologous to the

Abbreviations used: E6AP, E6-associated protein; HPV, human papillomavirus; MALDI-TOF, matrix assisted laser desorption ionization-time of flight; MS, mass spectrometry; HCV, hepatitis C virus; MAb, monoclonal antibody; PAb, polyclonal antibody; GAPDH, glyceraldehydes-3-phosphate dehydrogenase; CHX, cycloheximide.

T. Shimoji and K. Murakami contributed equally to this work.

Grant sponsor: Japan Health Sciences Foundation; Grant sponsor: Ministry of Health, Labor, and Welfare; Grant sponsor: Promotion of Fundamental Studies in Health Sciences of the National Institute of Biomedical Innovation (NIBIO), Japan.

*Correspondence to: Ikuo Shoji, MD, PhD, Division of Microbiology, Kobe University Graduate School of Medicine, 7-5-1 Kusunoki-cho, Chuo-ku, Kobe, Hyogo 650-0017, Japan. E-mail: ishoji@med.kobe-u.ac.jp

Received 26 November 2008; Accepted 14 January 2009 • DOI 10.1002/jcb.22096 • 2009 Wiley-Liss, Inc.

Published online 9 February 2009 in Wiley InterScience (www.interscience.wiley.com).

E6AP carboxyl terminus [Huibregtse et al., 1995]. Known substrates of the E6–E6AP complex include the tumor suppressor p53 [Scheffner et al., 1993], the PDZ domain-containing protein scribble [Nakagawa and Huibregtse, 2000] and NFX1-91, a transcriptional repressor of the gene encoding hTERT [Gewin et al., 2004]. Interestingly, E6AP is not involved in the ubiquitylation of p53 in the absence of E6 [Talis et al., 1998]. Several potential E6-independent substrates for E6AP have been identified, such as HHR23A and HHR23B (the human orthologs of *Saccharomyces cerevisae* Rad23) [Kumar et al., 1999], Blk (a member of the Src family kinases) [Oda et al., 1999], Mcm7 (which is involved in DNA replication) [Kuhne and Banks, 1998], trihydrophobin 1 [Yang et al., 2007], and AIB1 (a steroid receptor coactivator) [Mani et al., 2006].

Some patients with Angelman syndrome, a severe neurological disorder linked to E6AP, have mutations within the catalytic cleft that have been shown to reduce E6AP ubiquitin ligase activity [Kishino et al., 1997; Cooper et al., 2004]. Despite the significant progress in the study of Angelman syndrome-associated E6AP mutations, none of the identified E6AP substrates have been directly linked to the disorder. The physiological functions of E6AP are poorly understood at present.

In an attempt to identify novel substrates of E6AP, we identified annexin A1 (formerly known as lipocortin 1) as an E6AP-binding protein. Annexin A1 is a 37-kDa member of the annexin superfamily of Ca^{2+} and phospholipid-binding proteins [Lim and Pervaiz, 2007]. Annexin A1 is involved in the inhibition of cell proliferation, anti-inflammatory effects, and the regulation of cell differentiation. In addition, annexin A1 is involved in the regulation of cell death signaling, phagocytosis of apoptosis, and the process of carcinogenesis [Buckingham et al., 2006; Lim and Pervaiz, 2007]. Annexin A1 is phosphorylated by various kinases such as tyrosine kinase, pp60c-src [Varticovski et al., 1988], protein kinase C [Oudinet et al., 1993], epidermal growth factor receptor protein kinase [Haigler et al., 1987], and hepatocyte growth factor receptor kinase [Skouteris and Schroder, 1996].

In this study, we have examined the possibility that the stability of annexin A1 is regulated through E6AP-dependent ubiquitylation. Our study revealed that E6AP mediates ubiquitin-dependent degradation of annexin A1 in a Ca^{2+}-dependent manner. Our results raise the possibility that E6AP may have a role in controlling the diverse functions of annexin A1.

MATERIALS AND METHODS

CELL CULTURE AND TRANSFECTION

Human embryonic kidney (HEK) 293T cells, and human cervical carcinoma C33-A cells were cultured in Dulbecco's modified Eagle's medium (DMEM) (Sigma, St. Louis, MO) supplemented with 50 IU/ml penicillin, 50 μg/ml streptomycin (Invitrogen, Carlsbad, CA), and 10% (v/v) fetal bovine serum (FBS) (JRH Biosciences, Lenexa, KS) at 37°C in a 5% CO_2 incubator. HEK 293T cells and C33-A cells were transfected with plasmid DNA using FuGene 6 transfection reagents (Roche, Mannheim, Germany). The *Spodoptera frugiperda* (Sf) 9 cells were cultured in TC100 (JRH Biosciences) supplemented with 10% (v/v) FBS and 100 μg/ml kanamycin at 26°C in an incubator. The *Trichoplusia ni* (Tn) 5 cells were cultured in Ex-Cell 405 (JRH Biosciences) at 26°C in an incubator.

PLASMIDS AND RECOMBINANT BACULOVIRUSES

To express annexin A1 as a FLAG-tagged fusion protein in mammalian cells, annexin A1 fragment was amplified from pKK-trc-lipo-155 (a kind gift from Dr. Browning, Biogen) by polymerase chain reaction (PCR) using two oligonucleotides, 5′-TATCCCGG-GAACCACCATGGCAATGGTATCAGAATTCC-3′ and 5′-TATGCGG-CCGCTTACTTATCGTCGTCATCCTTGTAATCGTTTCCTCCACAAAG-AGCC-3′. The FLAG-tag sequence was fused to the C-terminus of the annexin A1 gene in frame. The amplified PCR fragment was digested with *Sma*I and *Not*I, purified, and subcloned into pCAGGS [Niwa et al., 1991], resulting in pCAG-annexin A1-FLAG. To express E6AP and the active-site cysteine-to-alanine mutant of E6AP in mammalian cells, pCAG-HA-E6AP isoform II and pCAG-HA-E6AP C-A were used [Shirakura et al., 2007]. The C-A mutation was introduced at the site of E6AP C843 [Kao et al., 2000]. To express Nedd4, pCAG-HA-Nedd4 was constructed. To make a fusion protein consisting of glutathione S-transferase (GST) fused to the N-terminus of E6AP in *Escherichia coli* (*E. coli*), pGEX-E6AP was used [Shirakura et al., 2007]. Recombinant baculoviruses expressing GST-E6AP were described previously [Shirakura et al., 2007]. To express hexahistidine (His)-tagged annexin A1 in *E. coli*, annexin A1 fragment was amplified from pKK-trc-lipo-155 by PCR using two oligonucleotides, 5′-TATCCCGGGAACCACCATGGCAATGG-TATCAGAATTCC-3′ and 5′-ATAGCGGCCGCGTTTCCTCCACAAA-GAGCC-3′. The PCR fragment was purified and digested with *Sma*I and *Not*I. pET21b was digested with *Nde*I, blunt ended with a DNA blunting kit (Takara, Japan), and digested with *Not*I. Then, the PCR fragment of annexin A1 was ligated into the pET21b fragment, resulting in pET21b-annexin A1. To map the E6AP-binding site on annexin A1 protein, a series of expression plasmids for GST-annexin A1 fusion proteins were constructed by amplifying annexin A1 gene fragments with PCR using sense primers containing *Sma*I site and antisense primers containing a *Not*I site. The amplified PCR fragments were subcloned into pGEM T-Easy (Promega, Madison, WI) and verified by sequencing. Then, the annexin A1 gene fragments were digested with *Sma*I and *Not*I and ligated into the *Sma*I–*Not*I site of pGEX 4T-1 (GE Healthcare, Uppsala, Sweden). The annexin A1 (1-41) gene fragment was amplified from pET21b-annexin A1 by PCR using two oligonucleotides, 5′-TATCCCGG-GAACCACCATGGCAATGGTATCAGAATTCC-3′ and 5′-ATATAGC-GGCCGCTTAGGTAGGATAGGGGCTCACCGCT-3′. The PCR primers used to amplify the annexin A1 fragments were as follows:

Annexin A1 (42–346): 5′-TATCCCGGGAACCACCATGTTCAAT-CCATCCTCGGATGTCG-3′ and 5′-ATATAGCGGCCGCTTAGTTT-CCTCCACAAAGAGCC-3′.
Annexin A1 (42–113): 5′-AAACCCGGGTATGTTCAATCCATCCT-CGGATGTCG-3′ and 5′-TTTGCGGCCGCTTATTTTAGCAGAGC-TAAAACAAC-3′.
Annexin A1 (114–195): 5′-AAACCCGGGTATGACTCCAGCG-CAATTTGATGC-3′ and 5′-TTTGCGGCCGCTTAATTCACACCAA-AGTCCTCAG-3′.

Annexin A1 (196–274): 5′-AAACCCGGGTATGGAAGACTTGG-CTGATTCAG-3′ and 5′-TTTGCGGCCGCTTAGCTTGTGGCGCAC-TTCACG-3′.
Annexin A1 (275–346): 5′-AAACCCGGGTATGAAACCAGCTTT-CTTTGCAGAG-3′ and 5′-ATATAGCGGCCGCTTAGTTTCCTCCA-CAAAGAGCC-3′.
Annexin A1 (42–195): 5′-AAACCCGGGTATGTTCAATCCATCC-TCGGATGTCG-3′ and 5′-TTTGCGGCCGCTTAATTCACACCAAA-GTCCTCAG-3′.
Annexin A1 (114–274): 5′-AAACCCGGGTATGACTCCAGCGCA-ATTTGATGC-3′ and 5′-TTTGCGGCCGCTTAGCTTGTGGCGCAC-TTCACG-3′.
Annexin A1 (196–346): 5′-AAACCCGGGTATGGAAGACTTGG-CTGATTCAG-3′ and 5′-ATATAGCGGCCGCTTAGTTTCCTCCAC-AAAGAGCC-3′.

The sequences of the inserts were extensively verified using an ABI PRISM 3100-Avant Genetic Analyzer (Applied Biosystems, Foster City, CA). To express GST, GST-E6AP, and MEF-E6AP in the baculovirus expression system, recombinant baculoviruses were recovered using a BaculoGold transfection kit (Pharmingen, San Diego, CA) as described previously [Shirakura et al., 2007].

ANTIBODIES

The mouse monoclonal antibodies (MAbs) used in this study were anti-HA MAb (12CA5) (Roche), anti-HA 16B12 MAb (HA.11; BabCO), anti-Annexin I MAb (BD Biosciences, San Jose, CA), anti-glyceraldehyde-3-phosphate dehydrogenase (GAPDH) MAb (Chemicon, Temecula, CA), anti-GST MAb (Santa Cruz Biotechnology, Santa Cruz, CA), anti-ubiquitin MAb (Chemicon), anti-E6AP MAb (E6AP-330) (Sigma), and anti-β-actin MAb (Ab-1) (Calbiochem, San Diego, CA). The polyclonal antibodies (PAbs) used in this study were anti-HA rabbit PAb (Y-11; Santa Cruz Biotechnology), anti-FLAG rabbit PAb (F7425; Sigma), anti-E6AP rabbit PAb (H-182; Santa Cruz Biotechnology), and anti-GST goat PAb (Amersham Bioscience, Buckinghamshire, UK).

IDENTIFICATION OF E6AP-BINDING PROTEINS WITH MALDI-TOF MASS SPECTROMETRY

To screen for potential E6AP-binding proteins, GST pull-down assays were performed using GST-E6AP and ten 225 cm^2-flasks (Corning, New York, NY) of confluent C-33A cells as the source of protein. The cells were lysed in 15 ml of the cell lysis buffer (100 mM Tris-HCl, pH 7.4, 100 mM NaCl, 0.5% Triton X-100 [ICE Biomedicals, Aurora, OH], Complete protease inhibitor cocktail [Roche]). The samples were incubated at 4°C for 1 h, and centrifuged at 13,000*g* for 30 min. The supernatants were collected and pre-cleared with 250 μl of 50% slurry glutathione-Sepharose 4B beads (Amersham Bioscience) to remove proteins that can nonspecifically bind to glutathione-Sepharose 4B beads. The supernatants were then pre-cleared with 250 μg of GST immobilized on glutathione-Sepharose 4B beads to remove proteins which can bind to GST. Then, the supernatant was collected, mixed with 250 μg of GST-E6AP or GST immobilized on glutathione-Sepharose 4B beads, and incubated for 1 h at 4°C. The beads were collected and washed with the cell lysis buffer three times. To remove the bound proteins from GST-E6AP, the bound proteins were released with the releasing buffer (10 mM Tris-HCl, pH 7.4, 150 mM NaCl, 1% sodium deoxycholate, 0.1% sodium dodecyl sulfate [SDS], 1% Triton X-100) five times. The released proteins were mixed with 20% (w/v) trichloroacetic acid (TCA) and incubated at 4°C for 30 min. After centrifugation, the TCA-precipitated samples were washed with ice-cold acetone four times, dried, and lysed in SDS-polyacrylamide gel electrophoresis (SDS-PAGE) loading buffer. The samples were separated by 7.5% SDS-PAGE and stained with Coomassie brilliant blue (CBB). The specific protein bands were excised from the gel and subjected to in-gel trypsin digestion. The tryptic peptide mixtures were analyzed by MALDI-TOF/MS analysis [Kaji et al., 2000]. Prior to MALDI-TOF/MS analysis, the peptide mixtures were desalted using C18 Zip Tips (Millipore, Bedford, MA) according to the manufacturer's instructions. The peptide data were collected in the reflection mode and with positive polarity, using a saturated solution of α-cyano-4-hydroxycinnamic acid (Sigma) in 50% acetonitrile (PE Biosystems, Foster City, CA) and 0.1% trifluoroacetic acid as the matrix. Spectra were obtained using a Voyger DE-STR MALDI-TOF mass spectrometer (PE Biosystems). The database-fitting program MS-Fit at the website (http://jpsl.ludwig.edu.au/ucsfhtml3.4/msfit.htm) of the University of California, San Francisco was used to interpret the MS spectra of the protein digests.

EXPRESSION AND PURIFICATION OF RECOMBINANT PROTEINS

E. coli BL21 (DE3) cells were transformed with plasmids expressing GST fusion protein or His-tagged protein and grown at 37°C. Expression of the fusion protein was induced by 1 mM isopropyl-β-D-thiogalactopyranoside at 25°C for 4 h. Bacteria were harvested, suspended in lysis buffer (phosphate-buffered saline [PBS] containing 1% Triton X-100, Complete protease inhibitor cocktail, EDTA free [Roche]), and sonicated on ice.

Hi5 cells were infected with the recombinant baculoviruses to produce GST-E6AP or GST. GST-E6AP and GST-fusion proteins were purified on glutathione-Sepharose beads (Amersham Bioscience) according to the manufacturer's protocols. His-tagged proteins were purified on Ni-NTA beads (Qiagen, Hilden, Germany) according to the manufacturer's protocols. MEF-E6AP and MEF-E6AP C-A [Shirakura et al., 2007] were purified on anti-FLAG M2 agarose beads (Sigma) according to the manufacturer's protocols.

IMMUNOPRECIPITATION AND IMMUNOBLOT ANALYSIS

Cells were lysed in IP buffer (100 mM Tris-HCl, 100 mM NaCl, pH 7.4, 0.5% Triton X-100, 0.5 mM $CaCl_2$, plus Complete protease inhibitor cocktail, EDTA free) at 4°C for 15 min. Extracts were clarified by centrifugation at 13,000*g* for 20 min, and soluble lysates were pre-cleared with protein G Sepharose (GE Healthcare). The samples were incubated with anti-FLAG M2 agarose (Sigma) and rotated at 4°C for 5 h. The beads were washed five times with IP buffer, and bound proteins were eluted with Laemmli sample buffer. Samples were separated by 10% SDS-PAGE. Immunoblot analysis was performed essentially as described previously [Harris et al., 1999]. The membrane was visualized with SuperSignal West Pico Chemiluminescent Substrate (Pierce, Rockford, IL).

IN VIVO UBIQUITYLATION ASSAY

In vivo ubiquitylation assays were performed essentially as described previously [Shirakura et al., 2007]. Where indicated, cells were treated with 25 μM MG132 (Calbiochem) or with dimethylsulfoxide (DMSO; control) for 30 min prior to collection. FLAG-annexin A1 was immunoprecipitated with anti-FLAG MAb. Immunoprecipitates were analyzed by immunoblotting, using either anti-HA PAb or anti-annexin A1 MAb to detect ubiquitylated annexin A1.

IN VITRO UBIQUITYLATION ASSAY

In vitro ubiquitylation assays were performed essentially as described previously [Shirakura et al., 2007]. For in vitro ubiquitylation of annexin A1, purified GST-annexin A1 was used as a substrate. Purified GST was used as a negative control. Assays were done in 40-μl volumes containing 20 mM Tris–HCl, pH 7.6, 50 mM NaCl, 5 mM ATP, 8 μg of bovine ubiquitin (Sigma), 0.1 mM DTT, 200 ng of mouse E1, 200 ng of E2 (UbcH7), and 0.5 μg of MEF-E6AP, in the presence or absence of $CaCl_2$ as indicated. The reaction mixtures were incubated at 37°C for 120 min followed by immunoblotting.

SIRNA TRANSFECTION

HEK 293T cells (3×10^5 cells in a 6-well plate) were transfected with 40 pmol of either E6AP-specific small interfering RNA (siRNA; Sigma), or scramble negative-control siRNA duplexes (Sigma) using HiPerFect transfection reagent (Qiagen) following the manufacturer's instructions. The E6AP-siRNA target sequences were as follows:

siE6AP-1 (sense) 5′-GGGUCUACACCAGAUUGCUTT-3′; scramble negative control (siCont-1) (sense) 5′-UUGCGGGUCUAAUCACCGATT-3′ [Shirakura et al., 2007]; E6AP-2 (sense), 5′-CAACUCCUGCUCUGAGAUATT-3′; and scramble negative control (siCont-2), 5′-AGACCUACCCGAUUACUGUTT-3′ [Kelley et al., 2005].

ANNEXIN A1 PROTEIN AND E6AP-BINDING ASSAYS

To map the E6AP binding site on annexin A1 protein, GST pull-down assays were performed. A series of recombinant GST-annexin A1 proteins were expressed in *E. coli* and purified using glutathione-Sepharose 4B beads. Equivalent amounts of purified proteins, as estimated by CBB staining, were used for the binding assays. For pull-down assays, purified MEF-E6AP was incubated with GST-annexin A1 proteins immobilized on glutathione-Sepharose 4B beads in 1 ml of the binding buffer (50 mM Tris–HCl [pH 7.4], 150 mM NaCl, 1% Triton X-100, and 5 mM $CaCl_2$) at 4°C for 4 h. The beads were washed four times with binding buffer, and the pull-down complexes were separated by SDS–PAGE on 10% polyacrylamide gels and analyzed by immunoblotting with anti-FLAG MAb.

CYCLOHEXIMIDE (CHX) HALF-LIFE EXPERIMENTS

To examine the half-life of annexin A1 protein, transfected HEK 293T cells were treated with 50 μg/ml CHX at 44 h post-transfection. The cells at time-point zero were harvested immediately after treatment with CHX. Subsequent time points were incubated in medium containing CHX at 37°C for 3, 6, and 9 h as indicated.

CONFOCAL IMMUNOFLUORESCENCE MICROSCOPY

Cells were transfected with pCAG-HA-E6AP C-A and pCAG annexin A1-FLAG using TransIT-LT1 (Takara) according to the manufacturer's instructions. Transfected cells grown on collagen-coated coverslips were washed with PBS, fixed with 4% paraformaldehyde for 30 min at 4°C, and permeabilized with PBS containing 2% FCS and 0.3% Triton X-100. Cells were incubated with anti-HA mouse MAb and anti-FLAG rabbit PAb as primary antibodies, washed, and incubated with Alexa Fluor 488 goat anti-mouse IgG (Molecular Probes, Eugene, OR) and Alexa 555 Fluor goat anti-rabbit IgG (Molecular Probes) as secondary antibodies. Then the cells were washed with PBS, mounted on glass slides, and examined with an LSM510 laser scanning confocal microscope (Carl Zeiss, Oberkochen, Germany).

RESULTS

IDENTIFICATION OF ANNEXIN A1 AS A BINDING PARTNER FOR E6AP

To identify novel substrates for E6AP, we screened for E6AP-binding proteins using pull-down experiments with GST-E6AP. Whole cell lysates from C33-A cells were prepared as described above and incubated with immobilized GST-E6AP or GST alone. After the separation of bound proteins by SDS–PAGE, CBB staining of the gels revealed at least 15 specific bands precipitating with the GST-E6AP. The protein bands were excised from the gel and subjected to in-gel trypsin digestion. The tryptic peptide mixtures were analyzed by MALDI-TOF/MS as described above. Masses obtained using MALDI-TOF were analyzed using the MS-Fit program. This procedure identified seven individual proteins (Fig. 1A,a–g), such as a heat shock protein and a translation elongation factor. One of these bands, migrating at 37 kDa (Fig. 1A,e), was identified as annexin A1 based on six independent MS spectra (Fig. 1B). To verify the interaction of annexin A1 with E6AP, we repeated the pull-down experiments by incubating immobilized GST-E6AP with lysate from C-33A cells. Immunoblot analysis confirmed the proteomic identification of annexin A1 (Fig. 1C).

IN VIVO INTERACTION BETWEEN ANNEXIN A1 AND E6AP

To determine whether the interaction between annexin A1 and E6AP could take place in vivo, annexin A1-FLAG expression plasmid was introduced into HEK 293T cells together with either HA-E6AP expression plasmid or HA-Nedd4 (another HECT domain ubiquitin ligase) [Staub et al., 1996] expression plasmid. A catalytically inactive form of E6AP in which the active site cysteine residue has been substituted with alanine (C843A) was used to avoid potential degradation of interacting proteins. Cells were lysed and annexin A1-FLAG was immunoprecipitated with FLAG-beads. As shown in Figure 2A, HA-E6AP but not HA-Nedd4 was co-immunoprecipitated with annexin A1-FLAG, indicating that E6AP actually interacts with annexin A1 in the cells. We confirmed that the active form of HA-E6AP was also coimmunoprecipitated with annexin A1-FLAG (data not shown).

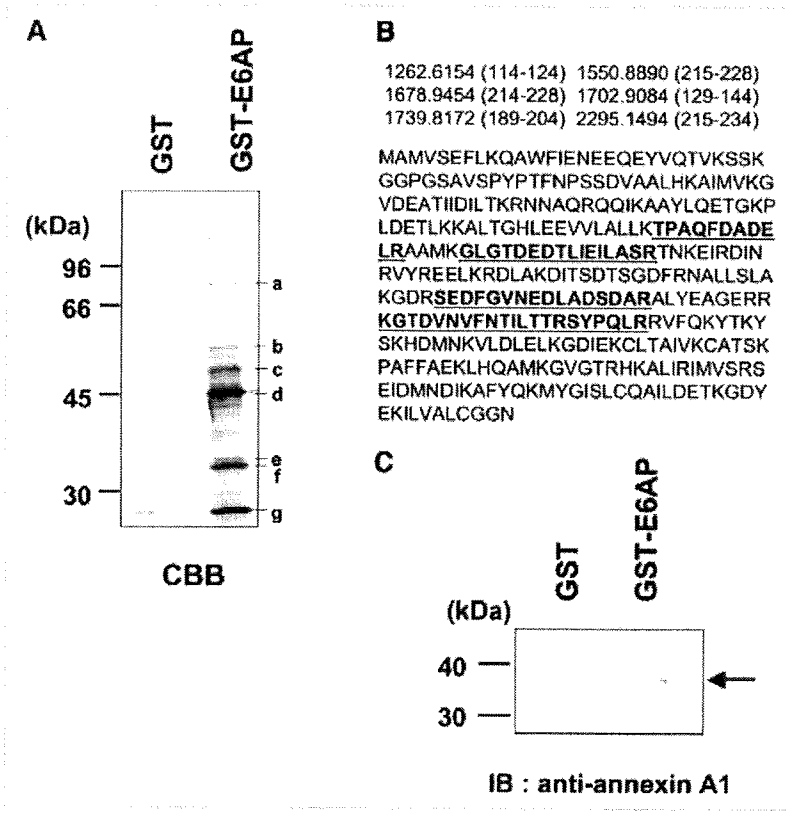

Fig. 1. Identification of annexin A1 as a binding partner for the E6AP. A: GST-E6AP on glutathione-Sepharose beads was incubated with whole-cell extract from C-33A cells. Bound proteins were detected by SDS–PAGE and CBB staining. Molecular weight markers are indicated, as well as the position of p37 (e), which likely corresponds to annexin A1. B: Peptide masses were identified by MALDI-TOF/MS and corresponding amino acids of annexin A1 (trypsin cleavage). Annexin A1 (accession no. 12654863) was identified through MALDI-TOF/MS as a candidate protein interacting with GST-E6AP. The database-fitting program MS-Fit was used to interpret the MS spectra of the protein digests. Six out of 22 masses obtained through the MALDI-TOF analysis corresponded to the theoretical values for annexin A1 cleavage (upper panel, amino acids corresponding to tryptic fragments in brackets) and represented 18% of the proteins' fragments (lower panel, peptides in bold print). The molecular weight search score, MOWSE, was 3.94E + 03. C: The identity of the band shown in panel A as annexin A1 was confirmed by Western blotting with anti-annexin A1 mouse MAb.

To determine whether annexin A1 and E6AP co-localize in the cells, immunofluorescence microscopy analysis was performed in two different cell lines, HEK 293T cells and C-33A cells. The immunofluorescence study showed that E6AP partially co-localized with annexin A1 in the cytoplasm of both types of cells (Fig. 2B).

To determine whether endogenous E6AP interacts with endogenous annexin A1 in vivo, C-33A cells were lysed and subjected to immunoprecipitation with anti-annexin A1 antibody or anti-E6AP antibody. Endogenous E6AP was co-immunoprecipitated with anti-annexin A1 antibody, but not with control antibody (Fig. 2C, left panel, upper lane). Moreover, endogenous annexin A1 was co-immunoprecipitated with anti-E6AP antibody, but not with control antibody (Fig. 2C, right panel, lower lane). These results suggest that endogenous E6AP can interact with endogenous annexin A1 in C-33A cells.

E6AP DECREASES STEADY-STATE LEVELS OF ANNEXIN A1 PROTEIN

To determine whether E6AP functions as an E3 ubiquitin ligase for the ubiquitylation of annexin A1, we assessed the effects of E6AP on annexin A1 protein in HEK 293T cells. The annexin A1-FLAG expression plasmid together with the plasmid for HA-tagged wild-type E6AP, catalytically inactive mutant E6AP, E6AP C-A, or Nedd4, was introduced into HEK 293T cells, and the levels of annexin A1 proteins were examined by immunoblotting. The steady-state levels of annexin A1 protein decreased with an increase of the E6AP plasmids (Fig. 3A,B). However, neither E6AP C-A nor Nedd4 decreased the steady-state levels of the annexin A1 protein, suggesting that E6AP enhances the degradation of annexin A1 protein.

E6AP ENHANCES THE DEGRADATION OF ANNEXIN A1 PROTEIN

To determine whether the E6AP-induced reduction of the annexin A1 protein is due to an increase in the rate of degradation of annexin A1 protein, we examined the degradation of annexin A1 using the protein synthesis inhibitor CHX. Annexin A1 together with wild-type E6AP or inactive mutant E6AP C-A was expressed in HEK 293T cells. At 44 h after transfection, the cells were treated with either 50 μg/ml CHX alone or 50 μg/ml CHX plus 25μM MG132 to inhibit

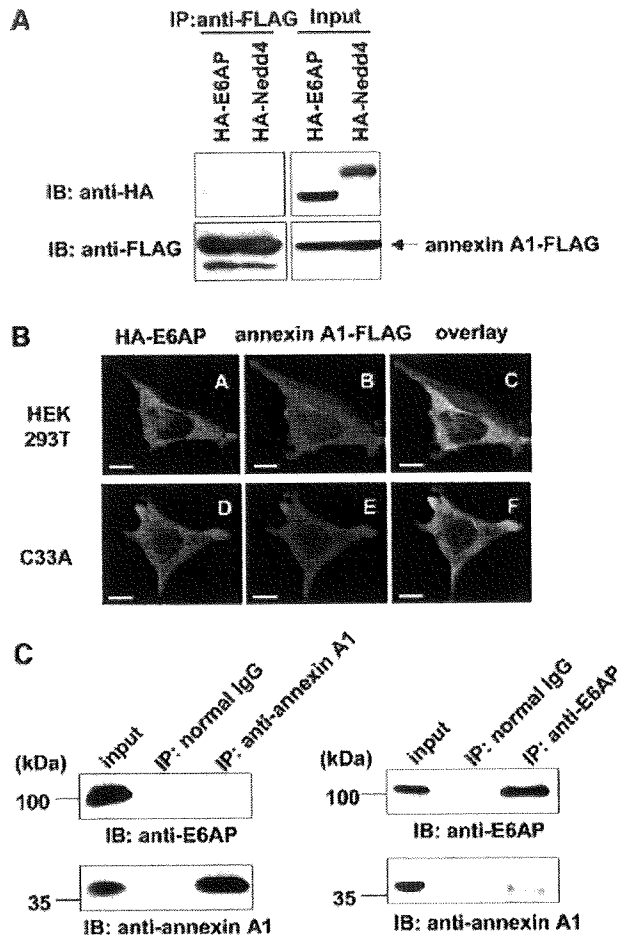

Fig. 2. In vivo interaction between annexin A1 and E6AP. A: HEK 293T cells were co-transfected with pCAG-annexin A1-FLAG together with pCAG-HA-E6AP C-A or pCAG-HA-Nedd4. The cell lysates were immunoprecipitated with FLAG beads and analyzed by immunoblotting with anti-HA PAb or anti-FLAG PAb. B: HEK 293T cells and C-33A cells were transfected with either HA-E6AP plasmid or annexin A1-FLAG plasmid, grown on coverslips, fixed, and processed for double-label immunofluorescence for HA-E6AP or annexin A1-FLAG. All the samples were examined with an LSM510 laser scanning confocal microscope (bar, 10 μm). C: C33A cells were lysed in the cell lysis buffer. The cell lysates were immunoprecipitated with anti-annexin A1 mouse MAb or control normal mouse IgG and analyzed with anti-E6AP mouse mAb or anti-annexin A1 mouse MAb as indicated (left panel). The cell lysates were immunoprecipitated with anti-E6AP mouse mAb or control normal mouse IgG and analyzed with anti-E6AP mouse mAb or anti-annexin A1 mouse mAb as indicated (right panel).

proteasome function. Cells were collected at 0, 3, 6, and 9 h following the treatment and analyzed by immunoblotting (Fig. 4A). Overexpression of E6AP resulted in rapid degradation of the annexin A1 protein, whereas the annexin A1 protein was stable in the cells transfected with inactive mutant E6AP C-A. Treatment of the cells with MG132 inhibited the degradation of annexin A1 (Fig. 4A). These results suggest that E6AP enhances proteasomal degradation of annexin A1.

KNOCKDOWN OF ENDOGENOUS E6AP BY SIRNA RESULTS IN ACCUMULATION OF ENDOGENOUS ANNEXIN A1 PROTEIN

To determine whether or not E6AP is critical for the degradation of endogenous annexin A1 protein, the expression of E6AP was knocked down by siRNA and the expression of annexin A1 and E6AP was analyzed by immunoblotting. We used two different siE6AP duplexes, siE6AP-1 and siE6AP-2, to knockdown the endogenous E6AP. Transfection of either siE6AP-1 or siE6AP-2 into HEK 293T cells resulted in a decrease in E6AP levels by 70–95% (Fig. 4B, the first panel), indicating that both siRNAs against E6AP resulted in a remarkable decrease in the protein level of E6AP. Knockdown of endogenous E6AP resulted in an accumulation of the endogenous annexin A1 protein, but no accumulation of the endogenous annexin A2 protein (Fig. 4B, the second and third panels), suggesting that the ubiquitylation and degradation of endogenous annexin A1 is specifically inhibited by knockdown of endogenous E6AP in vivo. These results suggest that endogenous E6AP plays a role in the proteolysis of endogenous annexin A1.

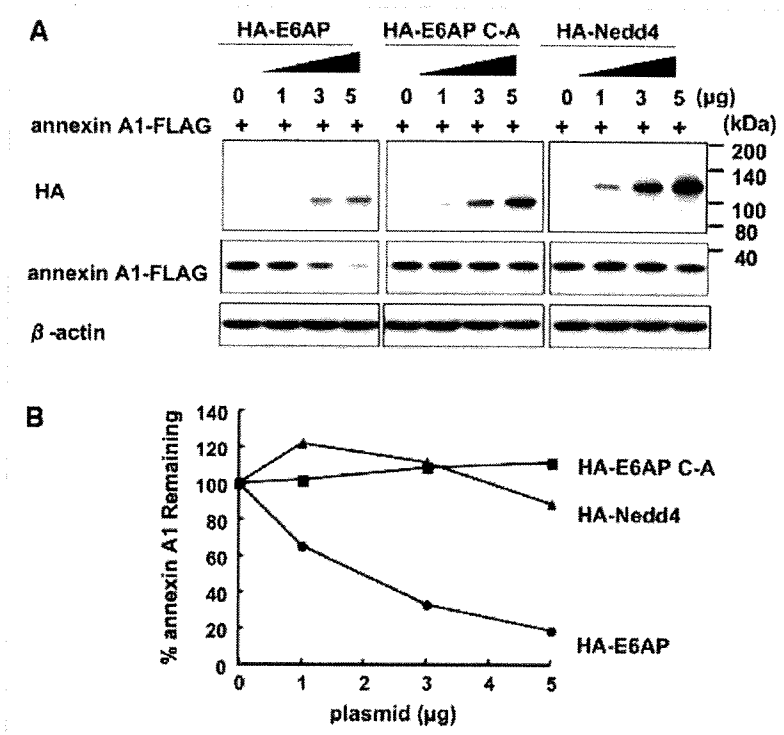

Fig. 3. E6AP decreases steady-state levels of annexin A1 protein in HEK 293T cells. HEK 293T cells (1×10^6 cells/10-cm dish) were transfected with 1 μg of pCAG annexin A1-FLAG along with either pCAG-HA-E6AP, pCAG-HA-E6AP C-A, or pCAG-HA-Nedd4 as indicated. At 48 h post-transfection, protein extracts were separated by SDS-PAGE and analyzed by immunoblotting with anti-HA PAb (top panel), anti-FLAG MAb (middle panel), and anti-β-actin MAb (bottom panel). B: Quantitation of data shown in panel A. Intensities of the gel bands were quantitated using the NIH Image 1.62 program. The level of β-actin served as a loading control. Circles, E6AP; squares, E6AP C-A; triangles, Nedd4.

E6AP MEDIATES UBIQUITYLATION OF ANNEXIN A1 IN VIVO

To determine whether E6AP can induce ubiquitylation of annexin A1 in cells, we performed in vivo ubiquitylation assays. HEK 293T cells were transfected with annexin A1-FLAG plasmid and either E6AP or Nedd4 plasmid, together with a plasmid encoding HA-tagged ubiquitin to facilitate the detection of ubiquitylated annexin A1 protein. Cell lysates were immunoprecipitated with anti-FLAG MAb and immunoblotted with anti-HA PAb to detect ubiquitylated annexin A1 protein. Only a faint ubiquitin signal was detected in the cells co-transfected with empty plasmid or Nedd4 plasmid (Fig. 5A, lanes 4 and 6). In contrast, co-expression of E6AP led to readily detectable ubiquitylated forms of the annexin A1 as a smear of higher-molecular-weight bands (Fig. 5A, lane 5). Immunoblot analysis with anti-FLAG PAb confirmed that annexin A1-FLAG proteins were immunoprecipitated and that higher-molecular-weight bands conjugated with HA-ubiquitin were indeed ubiquitylated forms of the annexin A1 proteins (Fig. 5B, lane 5). These results suggest that E6AP enhances ubiquitylation of annexin A1 in the cells.

E6AP MEDIATES UBIQUITYLATION OF ANNEXIN A1 IN VITRO

To reconstitute the E6AP-mediated ubiquitylation of annexin A1 in vitro, we performed an in vitro ubiquitylation assay of the annexin A1 using purified MEF-E6AP and GST-annexin A1 as described above. When the in vitro ubiquitylation reaction was carried out either in the absence of MEF-E6AP or in the presence of MEF-E6AP C-A, no ubiquitylation signal was detected (Fig. 5C, lanes 4 and 5). However, inclusion of purified MEF-E6AP in the reaction mixture resulted in ubiquitylation of GST-annexin A1 (Fig. 5C, lane 6), while no ubiquitylation was observed in the absence of ATP (Fig. 5C, lane 7). No signal was detected when GST was used as a substrate (data not shown). These results indicate that E6AP directly mediates ubiquitylation of annexin A1 protein in an ATP-dependent manner.

Ca^{2+}-DEPENDENT INTERACTION BETWEEN ANNEXIN A1 AND E6AP

We next assessed the effects of Ca^{2+} on the interaction between annexin A1 and E6AP. We performed the pull-down experiments by incubating immobilized GST-E6AP or GST alone with purified His-tagged annexin A1 in the presence or absence of 1 mM $CaCl_2$. After precipitation and SDS-PAGE, the bound annexin A1 was detected by immunoblotting with anti-annexin A1 antibody. GST-E6AP, but not GST, was able to precipitate annexin A1 only in the presence of Ca^{2+} (Fig. 6A, lane 4). These interactions were dependent on the concentration of Ca^{2+}, as increasing concentrations of Ca^{2+} resulted in an increase of binding of annexin A1 to E6AP (Fig. 6B). These

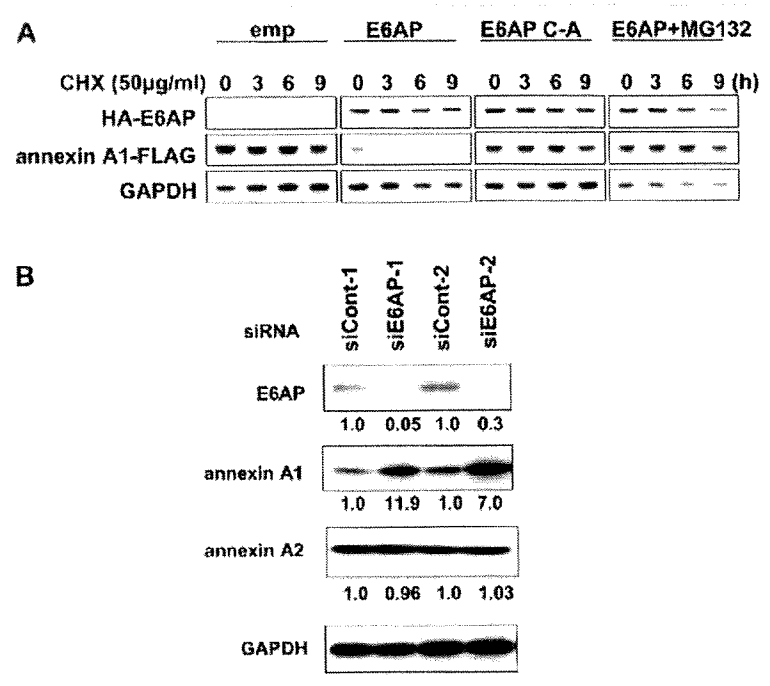

Fig. 4. E6AP-dependent degradation of annexin A1 protein. A: HEK 293T cells (1×10^6 cells/10-cm dish) were transfected with 1 μg of pCAG-annexin A1-FLAG plus 4 μg of empty vector, pCAG-HA-E6AP, or pCAG-HA-E6AP C-A. The cells were treated with 50 μg/ml CHX at 44 h after transfection. Cell extracts were collected at 0, 3, 6, and 9 h after treatment with CHX, followed by immunoblotting. Data are representative of three independent experimental determinations. B: Knockdown of endogenous E6AP by siRNA resulted in the accumulation of endogenous annexin A1 in HEK 293T cells. HEK 293T cells (3×10^5 cells/6-well plate) were transfected with 40 pmol of E6AP-specific duplex siRNA (or scramble negative control). Two sets of siRNAs (siE6AP-1 and siCont-1, siE6AP-2 and siCont-2) were used as described in Materials and Methods Section. The cells were harvested at 120 h after siRNA transfection. The relative levels of protein expression were quantitated using the NIH Image 1.62 program and are indicated below in the respective lanes. Data are representative of three independent experimental determinations.

results indicate that E6AP binds annexin A1 in a Ca^{2+}-dependent manner.

UBIQUITYLATION OF ANNEXIN A1 BY E6AP IS CA^{2+}-DEPENDENT

The HECT-type ubiquitin ligases transfer ubiquitin molecules to the substrates through direct interaction. Therefore, the E6AP-annexin A1 interaction is considered to be necessary for E6AP-mediated annexin A1 ubiquitylation. To determine if the molecular interaction is required for E6AP-mediated annexin A1 ubiquitylation, we performed in vitro ubiquitylation assay in the presence or absence of 1 mM $CaCl_2$. When in vitro ubiquitylation reaction was carried out in the presence of Ca^{2+}, the higher-molecular-weight species of GST-annexin A1 were detected with anti-GST PAb (Fig. 6C, lane 2), indicating that annexin A1 is polyubiquitylated by E6AP in vitro. However, no ubiquitylation signal was detected when the ubiquitylation reaction was carried out in the absence of Ca^{2+} (Fig. 6C, lane 1), indicating that the E6AP-annexin A1 interaction is required for E6AP-mediated annexin A1 ubiquitylation.

To further investigate whether the ubiquitylation of annexin A1 is dependent on the presence of Ca^{2+}, we examined the effects of EGTA on the E6AP-mediated ubiquitylation of annexin A1. Polyubiquitin chains were synthesized even in the presence of a high concentration of EGTA (Fig. 6D), indicating that E6AP was active even in the presence of EGTA. However, increasing amounts of EGTA resulted in decreases in the ubiquitylation of annexin A1 (Fig. 6E), suggesting that chelating the Ca^{2+} in the reaction mixture with EGTA inhibits the ubiquitylation of annexin A1. These findings suggest that the ubiquitylation of annexin A1 by E6AP is dependent on the presence of Ca^{2+}.

E6AP-BINDING DOMAIN FOR ANNEXIN A1 PROTEIN

To map the E6AP-binding domain on annexin A1 protein, GST pull-down assays were performed using a panel of annexin A1 deletion mutants expressed as GST-fusion proteins. Figure 7A shows a schematic representation of annexin A1 and known motifs in annexin A1. A series of deletion mutants of annexin A1 as GST fusion proteins (Fig. 7A) were expressed in *E. coli*. Purified MEF-E6AP was used to determine E6AP-binding domain. GST pull-down assays revealed that the core domain of annexin A1 (42-346), but not the N-terminal tail of annexin A1 (1-41), bound to E6AP (Fig. 7B, lanes 4 and 3). GST pull-down assays also showed that annexin A1 (114-274) and annexin A1 (196-346), but not annexin A1 (42-195), were able to bind to E6AP (Fig. 7B, lanes 5-7). As shown in Fig. 7C, GST-annexin A1 (196-274) bound to E6AP. These findings suggest that annexin repeat domain III is important for E6AP binding.